

## Rebounding Cores to Build Star Cluster Multiple Populations

G. PARMENTIER<sup>1</sup> AND A. PASQUALI<sup>1</sup>

<sup>1</sup>*Astronomisches Rechen-Institut, Zentrum für Astronomie der Universität Heidelberg, Mönchhofstr. 12-14, D-69120 Heidelberg, Germany*

(Accepted 2021 October 23)

### ABSTRACT

We present a novel approach to the riddle of star cluster multiple populations. Stars form from molecular cores. But not all cores form stars. Following their initial compression, such ‘failed’ cores re-expand, rather than collapsing. We propose that their formation and subsequent dispersal regulate the gas density of cluster-forming clumps and, therefore, their core and star formation rates. Clumps for which failed cores are the dominant core type experience star formation histories with peaks and troughs. In contrast, too few failed cores results in smoothly decreasing star formation rates. We identify three main parameters shaping the star formation history of a clump: the star and core formation efficiencies per free-fall time, and the time-scale on which failed cores return to the clump gas. The clump mass acts as a scaling factor. We use our model to constrain the density and mass of the Orion Nebula Cluster progenitor clump, and to caution that the star formation histories of starburst clusters may contain close-by peaks concealed by stellar age uncertainties. Our model generates a great variety of star formation histories. Intriguingly, the chromosome maps and O-Na anti-correlations of old globular clusters also present diverse morphologies. This prompts us to discuss our model in the context of globular cluster multiple stellar populations. More massive globular clusters exhibit stronger multiple stellar population patterns, which our model can explain if the formation of the polluting stars requires a given stellar mass threshold.

*Keywords:* galaxies: star clusters: general — stars: formation — ISM: clouds

### 1. INTRODUCTION

The presence of multiple stellar populations in star clusters remains a great riddle. Increasingly complex patterns have been revealed in the color-magnitude diagrams of Galactic globular clusters, which were once thought to epitomise simple stellar populations (see e.g. Milone et al. 2008; Anderson et al. 2009; Milone et al. 2015). These patterns stem from star-to-star abundance variations in He (Piotto et al. 2007), and in C, N and O (Milone et al. 2015). CNO abundance variations in individual globular clusters had already been identified by earlier spectroscopic studies (e.g. Kraft 1994), and Na-Mg-Al abundance variations are also common (Kraft 1994; Carretta et al. 2006; Charbonnel

2016, and references there in). These abundances are either correlated (Na-N-He) or anti-correlated (Na-O, N-C), which is the signature of hot-hydrogen burning (i.e. hydrogen-burning through the CNO-cycle and the NeNa- and MgAl-chains, Langer et al. 1993). The current consensus is that the low-mass stars enriched in Na-N-He and depleted in C and O formed out of gas polluted by the ejecta of stars massive enough to host hot-hydrogen burning. The nature of the polluters has remained debated, however. Candidate polluters include asymptotic giant branch stars (mass  $\simeq 4 - 8 M_{\odot}$ , D’Antona et al. 2002; D’Ercole et al. 2008; D’Antona et al. 2016), fast-rotating massive stars (mass  $> 20 M_{\odot}$ , Prantzos & Charbonnel 2006; Decressin et al. 2007), and super-massive stars (mass  $\simeq 10^4 M_{\odot}$ , Denissenkov & Hartwick 2014). Given their very different masses, measurements of stellar age spreads in globular clusters could help pinpoint the most likely scenario. Yet, this remains a challenging task, hin-

Corresponding author: Genevieve Parmentier  
gparm@ari.uni-heidelberg.de  
gparm@ari.uni-heidelberg.de

dered by the old age of globular clusters (Oliveira et al. 2020).

To complexify the picture further, the color-magnitude diagram of some younger clusters presents extended main sequence turn-offs, as well as split main sequences (for ages younger than 2 Gyr and 700 Myr, respectively). Observed in the Large Magellanic Cloud clusters and in open clusters of the Galactic disk, such features stem from different stellar rotation velocities (Dupree et al. 2017; Marino et al. 2018; Cordoni et al. 2018).

Last but not least, some forming clusters present stellar age distributions with peaks and troughs, suggesting that their star formation activity periodically recedes, to be re-invigorated later on. Examples are the Orion Nebular Cluster (ONC) in the Galactic disk (Beccari et al. 2017), and the young cluster R136 at the heart of the 30 Dor HII region in the Large Magellanic Cloud (Schneider et al. 2018). Interestingly, the age-span between successive peaks is of order 1 Myr for both the ONC and R136. It remains unclear whether and how these complex star formation histories relate to the multiple stellar populations of old globular clusters.

To explain the bumpy star formation history of the ONC, Kroupa et al. (2018) devise a scenario in which clusters with masses in the range  $600 - 20,000 M_{\odot}$  form at the converging point of molecular gas inflows. Newly-born O-stars shut off the inflow and star formation until they get ejected out of the cluster via stellar interactions. The gas inflow then resumes and builds the next stellar population.

We will explore another avenue, one in which the gas density of a cluster-forming clump is regulated by the formation and dispersal of 'failed' cores. Molecular cores are often considered the precursors of individual stars and small stellar systems (e.g. André et al. 2014; Ballesteros-Paredes et al. 2020, and references therein). Not all cores are prestellar, however. Some, possibly the majority, fail to form stars, 'bounce back' and disperse in the clump gas out of which they initially form (Taylor et al. 1996; Vázquez-Semadeni et al. 2005; Clark & Bonnell 2005; Gómez et al. 2007; Lada et al. 2008; Belloche et al. 2011a). The cycle of their formation and dispersal must therefore impact the mass and density of the clump gas, hence the core and star formation rates. We consider these 'failed'/'rebounding'/'dispersing' cores as a source of gas replenishment possibly leading to another star formation episode.

We will investigate whether different regions of the model parameter space can render different star formation histories, from sequences of fairly discrete star formation episodes to smoothly evolving star formation rates. Such a finding could be a major gateway to under-

stand the large variance observed in the multiple stellar populations of old globular clusters. Consider the distributions of stars along their O-Na anti-correlation (Carretta 2015; Charbonnel 2016) and in their chromosome map (Milone et al. 2017). They differ from cluster to cluster, being sometimes more clumpy, sometimes more continuous. Are the successive star formation episodes of some forming clusters (e.g. the ONC) the low-mass counterpart of the clumpy multiple stellar populations in some old globular clusters?

For a new star formation episode to rise, the previous one must first recede. We therefore opt for a model able to predict a decreasing star formation activity in cluster-forming clumps. We adopt the volume-density driven cluster-formation model of Parmentier & Pfalzner (2013), which predicts a star formation rate declining with time under the assumptions of constant clump mass and size. This decline is driven by two factors: (i) the decrease with time of the available gas mass due to ongoing star formation in an isolated constant-size clump, and (ii) the corresponding increase of the gas free-fall time (see Parmentier et al. 2014, for a detailed discussion). Evidence for decreasing star formation histories have been found for the Chamaeleon I molecular cloud (Luhman 2007; Belloche et al. 2011b) and, possibly, for the Perseus molecular cloud (Hatchell et al. 2005) (see also Preibisch 2012). Additionally, the amplitude of the three star formation episodes in the ONC is also a declining function of time (Beccari et al. 2017).

Parmentier & Pfalzner (2013) assume that the clump gas is directly converted into stars. Yet, stars form out of molecular cores, which are themselves condensations forming out of the clump gas. With this in mind, we add two major elements to their model: (1) the formation of cores constitute an intermediate stage in the conversion of the clump gas into stars, and (2) some cores - rather than collapsing and forming stars - re-expand into the clump gas reservoir, thereby re-supplying it in gas. In this preliminary study, we focus on cluster-forming clumps with uniform density.

The outline of the paper is as follow. In Sec. 2, we introduce a preliminary model, out of which we develop a criterion for the rise of a second star formation episode. Section 3 reviews the evidence for failed cores in simulations and observations of star-forming regions. In Sec. 4, we expand the model of Sec. 2 by differentiating between star-forming and failed cores, and we explore the parameter space in Sec. 5. We further upgrade the model in Sec. 6, where we relate the dissolution time-scale of the failed cores to the free-fall time of the host clump, using the Orion Nebula Cluster as a test-bed. In Sec. 7,

we discuss how our model star formation histories could be related to multiple stellar populations in old globular clusters, the limitations of our current model, and how an initial gas density gradient will impact our current results. We present our conclusions in Sec. 8.

## 2. MODEL FUNDAMENTALS

The model of [Parmentier & Pfalzner \(2013\)](#) predicts that the star formation rate of cluster-forming clumps is a decreasing function of time. This behavior stems from their model clumps having a constant radius and being isolated (i.e. no inflow, no outflow). Declining star formation rates such as those shown in Fig. 3 in [Parmentier et al. \(2014\)](#) and Fig. 4 in [Parmentier \(2019\)](#) define the first star formation episode of our model clumps. We aim at pinpointing the conditions leading to a second star formation episode, while retaining the assumptions of an isolated clump with a fixed size. The pivotal point here is: to form stars, a molecular clump must first form starless molecular cores. Some of these cores are bound, gravitationally unstable, collapse and form a star or a small stellar group (i.e. binary or triple). Not all cores are prestellar, however. Others remain unbound and eventually bounce back to the clump gas reservoir out of which they formed (e.g. [Taylor et al. 1996](#); [Vázquez-Semadeni et al. 2005](#); [Clark & Bonnell 2005](#); [Lada et al. 2008](#); [Belloche et al. 2011a](#), see also Sec. 3 for a discussion). The formation and dispersal of these 'failed' cores equates with removing some gas from the clump gas reservoir (core formation), and restoring it at a later time (core dispersal). When failed cores are abundant enough, their dispersal increases the leftover gas mass of a clump, renewing its core and star formation. To take into account the life-cycle of molecular cores - especially the non-collapsing ones - will therefore yield star formation histories different from those shown in [Parmentier et al. \(2014\)](#) and [Parmentier \(2019\)](#). In what follows, we coin *return time* the time-span needed for non-collapsing cores to disperse. The imprint of this parameter is the time-span between two successive peaks of a star formation history.

### 2.1. Building Bumpy Core Formation Histories

To model the core formation history of a cluster-forming clump, we use Eq. 18 of [Parmentier & Pfalzner \(2013\)](#), substituting the core formation rate per unit volume,  $d\rho_{\text{core}}(t)/dt$ , for the star formation rate per unit volume  $d\rho_{\text{star}}(t)/dt$ , and the core formation efficiency per free-fall time,  $\epsilon_{\text{ff,co}}$  for the star formation efficiency per free-fall time. We obtain

$$\frac{d\rho_{\text{core}}(t)}{dt} = \frac{\epsilon_{\text{ff,co}}}{\tau_{\text{ff}}(t)} \rho_{\text{gas}}(t) = \sqrt{\frac{32G}{3\pi}} \epsilon_{\text{ff,co}} \rho_{\text{gas}}(t)^{3/2}. \quad (1)$$

In this equation,  $\rho_{\text{gas}}(t)$  is the volume density of the clump gas at time  $t$  after core formation onset,  $\tau_{\text{ff}}(t)$  is the clump gas free-fall time and  $G$  is the gravitational constant. For a clear understanding of how the gas density impacts our model, we consider clumps with a uniform density. The evolution of clumps with an initial gas density gradient will be investigated in a future paper.

Equation 1 shows that the core formation rate per unit volume at a given time  $t$  depends on the corresponding gas density, hence on the gas mass inside a constant-radius clump. The gas mass equates with the clump total mass minus the mass in cores and stars. At first, ongoing core formation depletes the gas reservoir, thereby decreasing the core formation rate. The higher the initial density of the clump gas (i.e. the shorter its initial free-fall time  $\tau_{\text{ff},0}$ ) and/or the greater the core formation efficiency per free-fall time  $\epsilon_{\text{ff,co}}$ , the higher the initial core formation rate, but also the faster the gas density and core formation rate dwindle. We note that a gas density gradient would hasten the system evolution as well (see Fig. 4 in [Parmentier 2019](#)).

For a second core formation episode to occur, the core formation rate must stop declining and start rising. Eq. 1 shows that this happens if the clump gas reservoir is re-supplied in gas. In our model, this gas comes from cores formed at an earlier time, which now get dispersed following their failure to form stars. Consider cores formed at time  $t \gtrsim 0$  (shortly after core formation onset). After a return time  $t_{\text{return}}$ , a fraction  $f_{\text{return}}$  of the mass in cores returns to the clump gas. If the gas supply from dispersing cores overcomes the gas depletion due to ongoing core formation, the clump gas mass and density are on the rise. The return fraction  $f_{\text{return}}$  is obviously an important parameter. Here we can consider two extreme scenarios. If cores consist exclusively of non-collapsing ones, the return fraction is unity,  $f_{\text{return}} = 1$ . If only pre-stellar cores form, then the return fraction is their envelope mass fraction and  $f_{\text{return}} \simeq 2/3$  (i.e. the star formation efficiency of a single core is  $\simeq 1/3$ ; [Matzner & McKee 2000](#); [Alves et al. 2007](#)). We therefore adopt an intermediate value  $f_{\text{return}} = 0.85$ , and we keep it constant. For now, we assume that star-forming cores release their envelope and failed cores disperse on the same time-scale  $t_{\text{return}}$ . We will lift this hypothesis in Sec. 4. Armed with such a model, we can already anticipate the possibility of generating not just two, but multiple star formation episodes. Indeed, if the second core formation episode is significant enough, it will feed the emergence of a third one.

Having detailed how our preliminary model unfolds, we now consider a spherical clump of mass  $m_{\text{clump}}$  and

radius  $r_{clump}$ , and we infer the evolution with time of its gas density and core formation rate. The initial free-fall time of the clump gas is

$$\tau_{ff,0} = \sqrt{\frac{3\pi}{32G\rho_0}} \quad (2)$$

with  $\rho_0$  the clump volume density, equivalently the initial gas volume density:

$$\rho_0 = \rho_{gas}(t=0) = \frac{m_{clump}}{\frac{4}{3}\pi r_{clump}^3}. \quad (3)$$

The top panel of Fig. 1 shows as the solid red line the evolution of the gas density of a clump of mass  $m_{clump} = 10^4 M_\odot$ , radius  $r_{clump} = 1$  pc and core formation efficiency per free-fall time  $\epsilon_{ff,co} = 0.30$ . The return time and the return fraction of the core gas are set to  $t_{return} = 1$  Myr and  $f_{return} = 0.85$ . The return time is shown as the vertical dotted black line. These parameter values define the fiducial model of Fig. 1. As long as  $t < t_{return}$ , the evolution of the gas density is as predicted by Parmentier & Pfalzner (2013, their Eqs 17-18, written for cores rather than for stars). It steadily decreases due to the formation of new cores

$$\frac{d\rho_{gas}(t)}{dt} = -\frac{d\rho_{core}(t)}{dt}. \quad (4)$$

At  $t \gtrsim t_{return}$ , the gas density increases. This shows that the dispersal of cores returns enough mass to the clump gas to compensate for the gas used by ongoing core formation. The evolution of  $\rho_{gas}(t)$  already tells us that the core formation history will present two well distinct peaks followed by a third weaker one and a long trail of decreasing star formation activity.

How does modifying the fiducial model affect the time evolution of the gas density? We consider the following modifications (one at a time): a 10-times more massive clump ( $m_{clump} = 10^5 M_\odot$ ), a twice as small clump radius ( $r_{clump} = 0.5$  pc), a three-times smaller core formation efficiency per free-fall time ( $\epsilon_{ff,co} = 0.1$ ) and an (unphysically) small return fraction of the core mass ( $f_{return} = 0.3$ ). Results are presented along with the fiducial model in the top panel of Fig. 1.

Models with a reduced return fraction  $f_{return}$  (orange line) or a reduced core formation efficiency per free-fall time  $\epsilon_{ff,co}$  (green line) fail to replenish significantly the clump gas reservoir at  $t = t_{return}$ , either because of too great a mass fraction remaining locked inside cores (small  $f_{return}$ ), or because the gas density has not decreased enough to establish a strong gas density contrast between  $t = 0$  and  $t = t_{return}$  (small  $\epsilon_{ff,co}$ ).

In contrast, a higher initial gas density (obtained through either a larger clump mass  $m_{clump}$  or a smaller

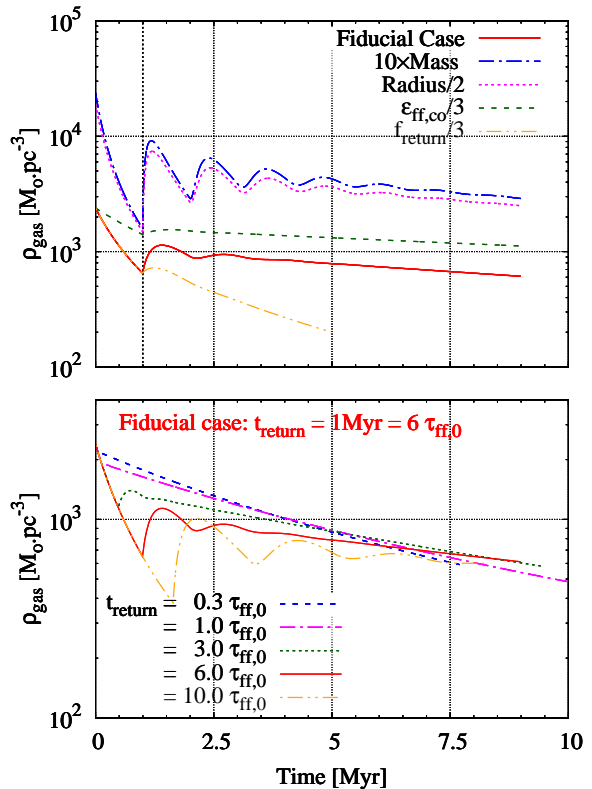


**Figure 1.** Evolution with time of the clump gas density. Top panel: Results for the fiducial model ( $m_{clump} = 10^4 M_\odot$ ,  $r_{clump} = 1$  pc,  $\epsilon_{ff,co} = 0.30$ ,  $t_{return} = 1$  Myr and  $f_{return} = 0.85$ : solid red line), for a ten-times more massive clump ( $m_{clump} = 10^5 M_\odot$ , dash-dotted blue line), for a twice as compact clump ( $r_{clump} = 0.5$  pc: dotted magenta line), for a three-times lower core formation efficiency per free-fall time ( $\epsilon_{ff,co} = 0.1$ : dashed green line), and for a  $\sim 3$ -times lower return fraction of the mass in cores ( $f_{return} = 0.3$ : dash-dotted orange line). Bottom panel: Results when varying the return time of the core mass:  $t_{return}/\tau_{ff,0} = 0.3, 1.0, 3.0, 6.0, 10.0$  (see key), all other parameters being identical to the top panel. The fiducial model (red line) is the same as in the top panel and corresponds to  $t_{return}/\tau_{ff,0} = 6.0$ . Note the different extents of the  $y$ -axis in both panels.

clump radius  $r_{clump}$ ) promotes the formation of successive star formation episodes. This is because the mass fraction of a clump which gets turned into cores depends on time in units of the free-fall time,  $t/\tau_{ff,0}$ . The physical return time of cores being fixed ( $t_{return} = 1$  Myr), the core return time  $t_{return}/\tau_{ff,0}$  is longer for denser clumps. This builds a stronger contrast between the gas densities at  $t = 0$  and  $t = t_{return}$  since the clump gas density is given a longer time-span  $t_{return}/\tau_{ff,0}$  to decrease. In turn, this allows the core gas released at  $t \gtrsim t_{return}$  to make a deeper impact.

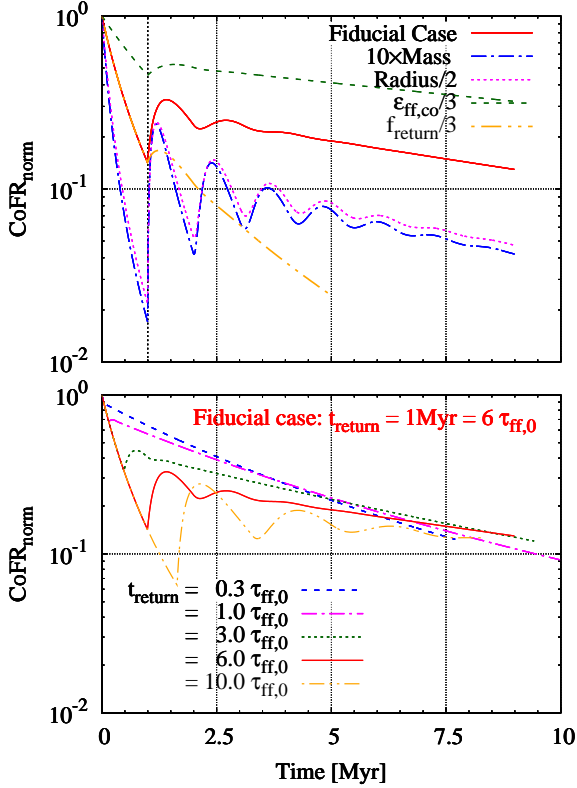


**Figure 2.** Same as Fig. 2 but for the core formation rates normalized to their initial value

The importance of the return time of failed cores is highlighted in the bottom panel of Fig. 1, where the fiducial model ( $\tau_{\text{ff},0} = 0.17 \text{ Myr}$  and  $t_{\text{return}} = 1 \text{ Myr} \equiv 6 \tau_{\text{ff},0}$ ) is compared to models with  $t_{\text{return}}/\tau_{\text{ff},0} = 0.3, 1.0, 3.0, 10.0$ . Clearly, longer return times  $t_{\text{return}}/\tau_{\text{ff},0}$  stimulate more core formation episodes.

Figure 2 shows the corresponding core formation rates normalized to their initial value (same model parameters and color-coding as in Fig. 1). The variations of the core formation rate are wider than those of the gas density, since the core formation rate scales as the gas density to the power of 1.5 (Eq. 1). Fig. 2 highlights the ability of our model to create very diverse core formation histories. This provides us with a hand to understand the strong variance observed in cluster multiple stellar populations, an aspect we shall discuss in Sec. 7.

The top panel of Fig. 2 may prompt us to conclude that dense and massive clumps are more likely to generate multiple core formation episodes. This conclusion is erroneous, however, and we will return to this important aspect also in Sec. 7. Here, we stress that the model parameters shaping a core formation history are the *dimensionless* parameters, namely, the core formation efficiency per free-fall time  $\epsilon_{\text{ff},\text{co}}$ , the return fraction

$f_{\text{return}}$  and return time  $t_{\text{return}}/\tau_{\text{ff},0}$  of the core mass. We now develop a tool to quantify their impact.

## 2.2. Criterion for a second core formation episode

The rise of a second core formation episode requires the gas density, in the aftermath of its steady decrease since core formation onset, to make an upturn and to start increasing at  $t = t_{\text{return}}$ . This is only doable if non-collapsing cores return to the clump gas a mass greater than that "pumped" to form new cores. Building on Eq. 1, the following equation expresses the clump gas density at  $t = t_{\text{return}} + dt$ ,  $\rho_{\text{gas}}(t_{\text{return}} + dt)$ , as a function of its counterpart at  $t = t_{\text{return}}$ ,  $\rho_{\text{gas}}(t_{\text{return}})$ :

$$\begin{aligned} \rho_{\text{gas}}(t_{\text{return}} + dt) &= \rho_{\text{gas}}(t_{\text{return}}) \\ &- \sqrt{\frac{32G}{3\pi}} \epsilon_{\text{ff},\text{co}} \rho_{\text{gas}}(t_{\text{return}})^{3/2} \cdot dt \quad (5) \\ &+ f_{\text{return}} \sqrt{\frac{32G}{3\pi}} \epsilon_{\text{ff},\text{co}} \rho_0^{3/2} dt. \end{aligned}$$

The second term on the right-hand side corresponds to the clump gas used by ongoing core formation. The third term accounts for the cores formed over the timespan  $[0, dt]$  that return to the clump gas over the time-interval  $[t_{\text{return}}, t_{\text{return}} + dt]$ . This third term depends on the clump initial gas density  $\rho_0$ , for this is the gas density at  $t = 0$  which dictates the formation rate of the cores being dispersed at  $t \gtrsim t_{\text{return}}$ . Following a few developments, we obtain the slope of the evolution with time of the gas density at  $t = t_{\text{return}}$ :

$$\begin{aligned} \left[ \frac{d\rho_{\text{gas}}(t)}{dt} \right]_{t=t_{\text{return}}} &= \frac{\rho_{\text{gas}}(t_{\text{return}} + dt) - \rho_{\text{gas}}(t_{\text{return}})}{dt} \\ &= \frac{CoFR(t=0)}{V} \cdot S(\epsilon_{\text{ff},\text{co}}, f_{\text{return}}, t_{\text{return}}/\tau_{\text{ff},0}) \quad (6) \end{aligned}$$

with

$$S(\epsilon_{\text{ff},\text{co}}, f_{\text{return}}, t_{\text{return}}/\tau_{\text{ff},0}) = \left[ f_{\text{return}} - \left( 1 + \frac{1}{2} \epsilon_{\text{ff},\text{co}} \frac{t_{\text{return}}}{\tau_{\text{ff},0}} \right)^{-3} \right] \quad (7)$$

In Eq. 6,  $V$  is the clump volume and  $CoFR(t=0)$  is the clump initial core formation rate:

$$\frac{CoFR(t=0)}{V} = \left[ \frac{d\rho_{\text{core}}(t)}{dt} \right]_{t=0} = \sqrt{\frac{32G}{3\pi}} \epsilon_{\text{ff},\text{co}} \rho_0^{3/2}. \quad (8)$$

The function  $S(\epsilon_{\text{ff},\text{co}}, f_{\text{return}}, t_{\text{return}}/\tau_{\text{ff},0})$ , given by Eq.7, determines whether the slope of  $\rho_{\text{gas}}(t)$  turns positive at  $t = t_{\text{return}}$ , or not. For instance, if the cores return no gas ( $f_{\text{return}} = 0$ ), then  $S < 0$  and

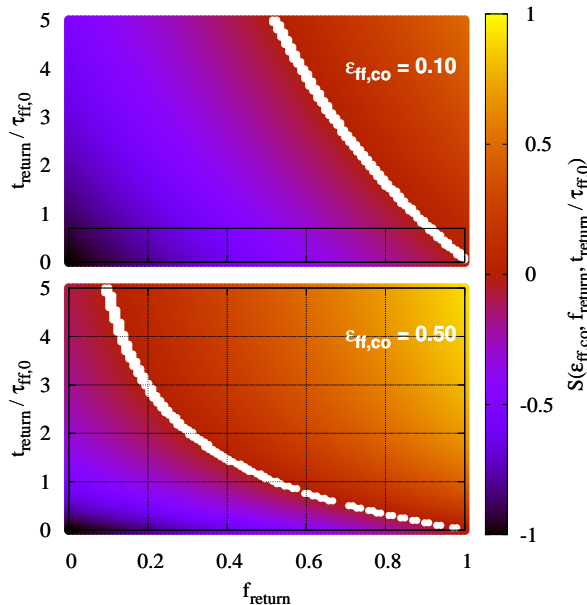


**Figure 3.** The  $S$ -function in dependence of the core formation efficiency per free-fall time  $\epsilon_{\text{ff,co}}$ , and of the return fraction  $f_{\text{return}}$  and return time  $t_{\text{return}}/\tau_{\text{ff},0}$  of the mass in cores (Eq. 7). It is color-coded according to the right-hand-side bar. When  $S > 0$  (red-to-yellow area), the clump gas density at  $t = t_{\text{return}}$  increases, possibly yielding a second core formation episode. When  $S < 0$  (red-to-black area), the clump gas density at  $t = t_{\text{return}}$  keeps decreasing, making impossible a second core formation episode. The white symbols depict the locus of points for which  $S = 0$ .

$\left[\frac{d\rho_{\text{gas}}(t)}{dt}\right]_{t=t_{\text{return}}} < 0$ . That is, the gas density keeps decreasing and there is no second core formation episode. Conversely, if  $S(\epsilon_{\text{ff,co}}, f_{\text{return}}, t_{\text{return}}/\tau_{\text{ff},0}) > 0$ ,  $t = t_{\text{return}}$  corresponds to the onset of a second core formation episode.

Figure 3 maps  $S(f_{\text{return}}, t_{\text{return}}/\tau_{\text{ff},0})$  for  $\epsilon_{\text{ff,co}} = 0.1$  and  $\epsilon_{\text{ff,co}} = 0.5$ . Its value is color-coded according to the right-hand-side bar, and the white symbols part the region for which  $S > 0$  from that with  $S < 0$ . When  $S > 0$  (red-to-yellow area), the clump gas gains, at  $t \gtrsim t_{\text{return}}$ , more mass from failed cores formed at  $t \gtrsim 0$  than it loses to ongoing core formation. When  $S < 0$  (red-to-black area), the formation of new cores consumes more clump gas than what failed cores provide. The higher the core formation efficiency per free-fall time, the wider the area of the  $(f_{\text{return}}, t_{\text{return}}/\tau_{\text{ff},0})$  parameter space for which  $S > 0$ . For a given core formation efficiency per free-fall time, a long return time of the core gas  $t_{\text{return}}/\tau_{\text{ff},0}$  and a large return mass fraction  $f_{\text{return}}$  favor a gas density increase at  $t = t_{\text{return}}$  and, therefore, an increase of the core formation rate. Such conclusions have already been suggested by Fig. 1.

We note that since, at core formation onset,

$$\left[\frac{d\rho_{\text{gas}}(t)}{dt}\right]_{t=0} = -\left[\frac{d\rho_{\text{core}}(t)}{dt}\right]_{t=0} = -\frac{CoFR(t=0)}{V}, \quad (9)$$

Eq. 6 can be rewritten as:

$$\left[\frac{d\rho_{\text{gas}}(t)}{dt}\right]_{t=t_{\text{return}}} = -\left[\frac{d\rho_{\text{gas}}(t)}{dt}\right]_{t=0} \times S(\epsilon_{\text{ff,co}}, f_{\text{return}}, t_{\text{return}}/\tau_{\text{ff},0}). \quad (10)$$

As can be seen,  $S$  compares how fast the gas density varies at  $t = t_{\text{return}}$  and  $t = 0$ . Since the upper limit on  $S$  is 1 (when  $f_{\text{return}} = 1$  and  $t_{\text{return}}/\tau_{\text{ff},0} \rightarrow \infty$ ), Eq. 10 expresses that, in absolute value, gas density variations at  $t \gtrsim t_{\text{return}}$  cannot be faster than those at  $t \gtrsim 0$ .

The model parameters promoting a second core formation episode are a high core formation efficiency per free-fall time  $\epsilon_{\text{ff,co}}$ , a large mass fraction  $f_{\text{return}}$  of core gas not ending into stars, and a long return time of the core gas to the clump gas  $t_{\text{return}}/\tau_{\text{ff},0}$ . A second core formation episode can be compared to a bouncing ball. A ball bounces back if (1) it is dropped from a high height, and (2) its encounter with the ground is as elastic as possible, such that it does not lose much of the kinetic energy accumulated through its initial fall. The height equivalent in our model is  $\epsilon_{\text{ff,co}} t_{\text{return}}/\tau_{\text{ff},0}$ , which determines which fraction of the clump mass has been turned into cores at  $t = t_{\text{return}}$ : the higher  $\epsilon_{\text{ff,co}}$ , the longer  $t_{\text{return}}/\tau_{\text{ff},0}$ , the greater the initial gas mass fraction turned into cores, and the more the gas density has dropped compared to its initial value. As for our  $f_{\text{return}}$  return fraction, its bouncing ball counterpart is the near-conservation of the ball kinetic energy: the higher  $f_{\text{return}}$ , the higher the core gas mass released at  $t = t_{\text{return}}$ , and the higher the gas density and core formation rate - like the ball - bounce back.

The high core formation efficiencies per free-fall time required for multiple core formation episodes (e.g.  $\epsilon_{\text{ff,co}} = 0.30$ ) are to be contrasted with the star formation efficiencies per free-fall time measured in the Galactic disk. The latter are of order one per cent (Krumholz & Tan 2007; Pokhrel et al. 2021). Given that individual star-forming cores have a star formation efficiency of  $\simeq 1/3$  (Matzner & McKee 2000; Alves et al. 2007), the formation efficiency per free-fall time of prestellar cores should not exceed a few per cent. Multiple core formation episodes therefore require non-collapsing cores to dominate the core population. This is also indicated by our high return fraction ( $f_{\text{return}} = 0.85$ ). We now review the evidence for significant populations of failed cores in molecular gas clouds, as found by observations and simulations.

### 3. EVIDENCE FOR FAILED CORES IN MOLECULAR CLOUDS

Belloche et al. (2011a) map the nearby molecular cloud Chamaeleon I in dust continuum emission at  $870\mu\text{m}$ . They find that 17% of its starless cores have a mass higher than the critical Bonnor-Ebert mass<sup>1</sup>. That is, only a minority of the Chamaeleon I cores are gravitationally unstable, and they tend to be the most massive ones. Additionally, the mass function of the starless cores is over-populated at its low-mass end, while being consistent with the Salpeter (1955) slope at the high-mass end. Belloche et al. (2011a) therefore conclude that most starless cores in Chamaeleon I are not prestellar. Belloche et al. (2011b) further suggest that some of these low-mass gravitationally-stable cores may never reach their critical mass and "get dispersed" in the future. Their interpretation is supported by a number of numerical simulations.

According to Clark & Bonnell (2005), most of the clumps (their terminology for cores) produced by supersonic turbulence are unbound. In one of their simulations, unbound clumps outnumber bound ones by two orders of magnitude. Unbound clumps/cores tend to be the low-mass ones, while prestellar cores are the most massive ones (since they have to reach the Jeans mass in the first place). A consequence of this is the absence of a one-to-one mapping from cores to stars and, therefore, from the core mass function to the stellar initial mass function (Klessen 2001; Clark & Bonnell 2005).

The nearby Pipe molecular cloud presents us with yet another population of failed cores. 159 cores with a mean volume density  $\simeq 7 \cdot 10^3 \text{ cm}^{-3}$  are detected by Lada et al. (2008). A comparison of their escape velocity with their - mostly thermal - gas velocity dispersion show most of them to be unbound (Lada et al. 2008, their fig. 4). The transition between the bound and unbound regimes occurs at a core mass of  $2 - 3 M_{\odot}$ , with 140 cores being less massive than  $3 M_{\odot}$ . Unless they experience a decrease of their internal pressure, or an increase of their external pressure (or a combination of both), such cores are unlikely to be prestellar. Lada et al. (2008) stress that unbound cores should persist for one or more sound crossing-times before they disperse in their surroundings (see also Keto et al. 2006). The radius of the unbound cores is of order  $0.075 \text{ pc}$  (Lada et al. 2008, their Fig. 6) and the sound speed in an isothermal gas at a temperature of  $10\text{K}$  is

$c_s = 0.2 \text{ km} \cdot \text{s}^{-1}$ . The sound crossing time of the unbound cores is therefore  $\tau_{\text{core,cross}} = 2 \cdot 0.075 \text{ pc} / (0.2 \text{ pc} \cdot \text{Myr}^{-1}) \simeq 0.75 \text{ Myr}$ . Unbound cores in the Pipe cloud should thus persist as coherent entities for about  $1 \text{ Myr}$ , possibly more (Lada et al. 2008).

Based on MHD simulations, Vázquez-Semadeni et al. (2005) too find that some cores/clumps form and dissolve later on. Considering a turbulent isothermal molecular cloud with a mean number density  $n_0 = 500 \text{ cm}^{-3}$ , they infer a life-expectancy of  $0.5$  to  $3.0 \text{ Myr}$  for its non-collapsing cores, similar to what Lada et al. (2008) estimate for the Pipe cloud cores. Note that the simulated cloud and the Pipe cloud have mean densities within an order of magnitude of each other (the mean density of the Pipe cloud is  $\simeq 100 \text{ cm}^{-3}$ , Kainulainen et al. 2014).

The life-expectancy of failed cores equates with the return time  $t_{\text{return}}$  of our preliminary model and, therefore, with the periodicity with which a clump unfolds its successive star formation episodes. Both Vázquez-Semadeni et al. (2005) and Lada et al. (2008) estimate this life-expectancy to be of order  $1 \text{ Myr}$ . Interestingly, this is similar to the time-span separating the three stellar populations of the ONC (Beccari et al. 2017, their Fig. 6), and Fig. 5 of Schneider et al. (2018) reveals a similar periodicity for the R136 cluster in  $30 \text{ Dor}$ . We shall come back to this in Sec. 6.

### 4. FAILED- VERSUS STAR-FORMING CORES

The preliminary model of Section 2 assumes that star-forming and failed cores release their gas on the same time-span  $t_{\text{return}}$ . Yet, both types of core evolve on different time-scales. First, Vázquez-Semadeni et al. (2005) stress that the re-expansion of failed cores is slower than their initial compression, as a result of self-gravity. Second, their MHD simulations show that failed cores are often less dense than prestellar ones, implying a longer free-fall time. Therefore, for at least two reasons (self-gravity and longer free-fall time), failed cores evolve more slowly than star-forming ones. This will help us meet one of the criteria unveiled in Sec. 2, namely, that failed cores should have long return times  $t_{\text{return}}/\tau_{\text{ff},0}$  to stimulate a second core formation episode. In this section, we assign different time-scales and different return fractions to failed and star-forming cores. In the case of star-forming cores, their envelope is the mass they return to their surroundings (Matzner & McKee 2000).

We assume that collapsing/star-forming cores have a mean density two orders of magnitude higher than that of their host clump. Their free-fall time  $\tau_{\text{ff,colco}}$  is thus ten times shorter than the clump's:  $\tau_{\text{ff,colco}} = 0.1\tau_{\text{ff},0}$ . Their lifetime ranges from one to ten times their

<sup>1</sup> The Bonnor-Ebert mass is the critical mass beyond which isothermal cores cannot be in hydrostatic equilibrium and collapse (Bonnor 1956; Tan et al. 2014).

free-fall time, depending on the magnetic field (e.g. Vázquez-Semadeni et al. 2005; Galván-Madrid et al. 2007; Ward-Thompson et al. 2007, and references therein). We therefore assume that the time-span between the formation of prestellar cores and the release of their envelope is 3 times their free-fall time. This defines the return time of their envelope to the clump gas as

$$t_{ret,colco} = 3\tau_{ff,colco} = 0.3\tau_{ff,0} . \quad (11)$$

Models yielding multiple core and star formation episodes hinge on failed cores outnumbering star-forming ones (see Fig. 3 and below). The exact values of the density contrast between star-forming cores and their host clump and of  $t_{ret,colco}/\tau_{ff,0}$  are thus minor issues.

As for the return time of the failed cores, namely, the time-span on which they re-expand into their surroundings, we fix it to 1 Myr (see Sec. 3):

$$t_{ret,fco} = 1 \text{ Myr} . \quad (12)$$

We will lift this assumption in Sec. 6, a single physical return time  $t_{ret,fco} = 1 \text{ Myr}$  for failed cores being an oversimplification, especially when considering very different host clump densities  $\rho_0$ .

Let us now quantify the core mass fractions (i.e. return fractions) associated to the return times defined above. We introduce the star formation efficiency per free-fall time  $\epsilon_{ff,st}$  in our model and derive the return fractions as a function of  $\epsilon_{ff,co}$  and  $\epsilon_{ff,st}$ . The mass  $dm_{co}(t)$  in cores formed over a time interval  $[t, t + dt]$  consists of three components: (1,2) stars and envelopes formed and released, respectively, by star-forming cores, and (3) failed cores. The following set of equations relates the mass fraction of failed cores,  $F_{fco}$ , to the mass fractions of envelopes and stars from star-forming cores,  $F_{env}$  and  $F_*$ , respectively:

$$1 = F_{fco} + F_* + F_{env} . \quad (13)$$

$$F_{env} = 2F_* . \quad (14)$$

$$\frac{\epsilon_{ff,st}}{\epsilon_{ff,co}} = F_* \quad (15)$$

For star-forming cores, we assume that the mass of their envelope is twice the mass of their stars (Eq. 14), i.e. the star formation efficiency of a star-forming core is one-third (Matzner & McKee 2000; Alves et al. 2007). Eq. 15 quantifies which fraction  $F_*$  of the total mass in cores eventually ends into stars. We define it as the ratio of the star formation efficiency per free-fall time  $\epsilon_{ff,st}$  of

**Table 1.** Mass fractions of the stars ( $F_*$ ) and envelopes ( $F_{env}$ ) from star-forming cores, and of the failed cores ( $F_{fco}$ ), for given  $\epsilon_{ff,co}$  and  $\epsilon_{ff,st}$ .

| $\epsilon_{ff,co}$         | $F_*$ | $F_{env}$ | $F_{fco}$ |
|----------------------------|-------|-----------|-----------|
| $\epsilon_{ff,st} = 0.01$  |       |           |           |
| 0.030                      | 0.33  | 0.67      | 0.00      |
| 0.100                      | 0.10  | 0.20      | 0.70      |
| 0.300                      | 0.03  | 0.07      | 0.90      |
| 0.500                      | 0.02  | 0.04      | 0.94      |
| $\epsilon_{ff,st} = 0.026$ |       |           |           |
| 0.078                      | 0.333 | 0.667     | 0.000     |
| 0.300                      | 0.087 | 0.173     | 0.740     |
| 0.500                      | 0.052 | 0.104     | 0.844     |

the host clump to its core formation efficiency per free-fall time  $\epsilon_{ff,co}$ . Note that  $\epsilon_{ff,co}$  accounts for all cores, both failed and star-forming ones. For an assumed pair  $(\epsilon_{ff,co}, \epsilon_{ff,st})$ , the above system of equations yields the respective contributions of stars, star-forming core envelopes, and failed cores to the core mass  $dm_{co}(t)$  formed over the time-span  $[t, t + dt]$ . Note that in Sec. 2.2,  $\epsilon_{ff,co}$  and  $f_{return}$  were independent of each other. With the above set of equations and a fixed  $\epsilon_{ff,st}$ ,  $\epsilon_{ff,co}$  and  $F_{fco}$  are now tied to each other, an increase of  $\epsilon_{ff,co}$  implying an increase of  $F_{fco}$ .

Table 1 provides examples for various core formation efficiencies per free-fall time  $\epsilon_{ff,co}$  and for  $\epsilon_{ff,st} = 0.01$  (Krumholz & Tan (2007); see also Fig. 4 in Parmentier & Pasquali (2020)) and  $\epsilon_{ff,st} = 0.026$  (Pokhrel et al. 2021). When  $\epsilon_{ff,st} = 0.01$  and  $\epsilon_{ff,co} = 0.03$  (or when  $\epsilon_{ff,st} = 0.026$  and  $\epsilon_{ff,co} = 0.078$ ), failed cores make no contribution to the core mass budget (since  $F_* = \epsilon_{ff,st}/\epsilon_{ff,co} = 1/3$  implies  $F_{env} = 2/3$  and  $F_{fco} = 0$ ). In the absence of failed cores, the only gas returned to the intra-cluster medium is that of star-forming core envelopes, which, per clump free-fall time, amounts to a few per cent of the clump gas (i.e. twice the star formation efficiency per free-fall time). This is an extremely small fraction compared to the  $\gtrsim 90\%$  of the clump mass which, per free-fall time, remain in its gas reservoir. Unsurprisingly, a model with no failed cores fails to generate multiple peaks in the core formation history (see below). As the core formation efficiency per free-fall time  $\epsilon_{ff,co}$  increases - while retaining the same star formation efficiency per free-fall time  $\epsilon_{ff,st}$  - the contribution of star-forming cores  $F_{env} + F_*$  dwindles, while that of failed cores  $F_{fco}$  rises (see Table 1).

The four cases of Table 1 with  $\epsilon_{ff,st} = 0.01$  are illustrated in Fig. 4. The mass and radius of the model



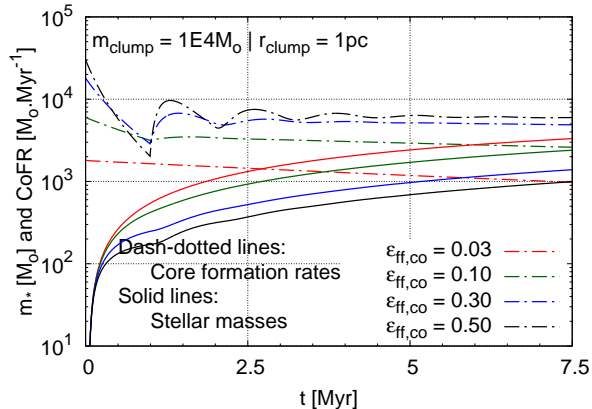


**Figure 4.** Evolution with time of the core formation rate (dash-dotted lines) and stellar mass (solid lines) of a clump with an initial gas mass  $m_{clump} = 10^4 M_{\odot}$ , a radius  $r_{clump} = 1$  pc and a star formation efficiency per free-fall time  $\epsilon_{ff,st} = 0.01$ . With higher core formation efficiencies per free-fall time  $\epsilon_{ff,co}$ , failed cores contribute more to the core mass budget (see Table 1), and multiple peaks get carved in the core formation history

clump are  $m_{clump} = 10^4 M_{\odot}$  and  $r_{clump} = 1$  pc, respectively, yielding an initial free-fall time  $\tau_{ff,0} = 0.167$  Myr for the clump gas. The return times of the core gas to the intra-cluster medium are as given by Eqs 11 ( $t_{ret,colco} = 0.3\tau_{ff,0} = 0.05$  Myr) and 12 ( $t_{ret,fco} = 1$  Myr  $= 6\tau_{ff,0}$ ). Dash-dotted and solid lines show the time evolutions of the core formation rate and of the stellar mass, respectively. Note that stellar masses start rising at  $t = t_{ret,colco}$ , that is, when the first stars emerge from their gaseous cocoon.

A higher core formation efficiency per free-fall time yields a higher core formation rate initially, but also a faster decrease of this one since the greater gas fraction trapped in cores reduces the clump gas mass accordingly. An increasingly steeper gas density gradient inside clumps would produce a similar effect (Fig. 4 in Parmentier 2019). At  $t \gtrsim t_{ret,fco} = 1$  Myr, i.e. after one return time of the failed cores, the core formation rate may make an upturn, a rise borne by the gas supplied by the failed cores formed at  $t \gtrsim 0$  Myr. The reasons as to why larger  $\epsilon_{ff,co}$  drive more star formation episodes is two-fold: (1) as in Sec. 2.2, a larger  $\epsilon_{ff,co}$  implies a greater decrease of the gas density after a given time-span  $t/\tau_{ff,0}$  (that is, the bouncing ball is dropped from a greater height), and (2) larger  $\epsilon_{ff,co}$  with a fixed star formation efficiency per free-fall time  $\epsilon_{ff,st}$  implies greater return fractions from failed cores (see Table 1; that is, the ball retains more of its kinetic energy while bouncing). These two effects can be visualized in Fig. 3 as (1) a widening of the region for which  $S > 0$  (i.e. the

white symbols and the red-to-yellow area are brought downwards for increasing  $\epsilon_{ff,co}$ ), and (2) an increase of  $f_{return}$  (i.e. moving to the right of the horizontal axis).

That a higher core formation efficiency per free-fall time is more likely to generate successive core formation episodes comes at a cost, however: higher  $\epsilon_{ff,co}$  yield lower stellar masses at any given time  $t$  (see solid lines in Fig. 4). This reduced star formation efficiency reflects the larger mass in failed cores produced for higher  $\epsilon_{ff,co}$ , and the correspondingly lower gas masses available for further core formation. This effect is not tremendous as increasing  $\epsilon_{ff,co}$  by a factor of 17 (i.e.  $0.50/0.03$ ) reduces stellar masses and star formation efficiencies by a factor  $\simeq 3$ .

## 5. PEAK NUMBER, GAS DENSITY AND CORE FORMATION EFFICIENCY

The color-magnitude diagram of the ONC presents 3 well-defined pre-main sequences, possibly suggesting three stellar populations with an age separation of about 1 Myr (Beccari et al. 2017). That is, the ONC would have experienced three successive core and star formation episodes. Building on the model refined in the previous section, we now explore which core formation efficiency per free-fall time  $\epsilon_{ff,co}$  and which initial gas density  $\rho_0$  are required to carve peaks in the star formation history of a clump with an imposed periodicity of 1 Myr. The results will be used in the next section to constrain the properties of the gaseous progenitor of the ONC based on its observed star formation history.

We test three core formation efficiencies per free-fall time, namely,  $\epsilon_{ff,co} = 0.1, 0.3, 0.5$ . The star formation efficiency per free-fall time is fixed, and we adopt  $\epsilon_{ff,st} = 0.01$ . The corresponding core mass fractions converted into stars ( $F_*$ ) and released to the clump gas as failed cores ( $F_{fco}$ ) are given in Table 1. As for the clump initial gas density, we test values ranging from  $\rho_0 = 10^2$  to  $10^5 M_{\odot} \cdot pc^{-3}$  in logarithmic steps of 1. The lower bound is of order the current mean density of the ONC, namely,  $4500 M_{\odot}$  of stars and gas enclosed within a radius of 2 pc (Hillenbrand & Hartmann 1998). The upper bound corresponds to the density of the "ultra-high density material" mapped at pc-scale by Hacar et al. (2020) in the active star-forming cloud OMC-1, located in the vicinity of the ONC. Densities in the range  $10^4 - 10^5 M_{\odot} \cdot pc^{-3}$  are also those characterizing the central regions of starburst clusters in the Galactic disk (e.g. Westerlund 1 and NGC 3603; see top panel of Fig. 10 in Parmentier et al. 2014). To vary the clump density, we vary its mass  $m_{clump}$  while keeping its radius  $r_{clump}$  constant. We assume  $r_{clump} = 2$  pc, which is approximately the current ONC radius (Hillenbrand & Hartmann 1998;

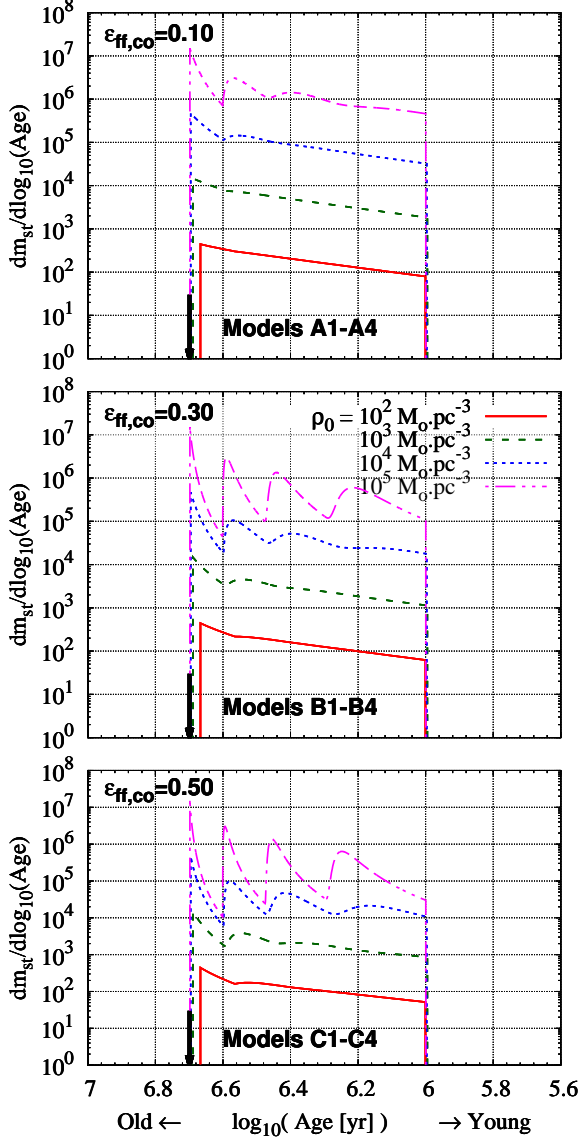


**Figure 5.** Logarithmic stellar age distributions for 3 core formation efficiencies per free-fall time (from top to bottom panel:  $\epsilon_{\text{ff,co}} = 0.1, 0.3, 0.5$ ), and 4 initial gas volume densities  $\rho_0$  (see key in middle panel). The adopted densities are representative of cluster-forming regions of the Galactic disk. Model parameters are provided in Table 2.

Da Rio et al. 2017). The corresponding clump masses are given in Table 2. All models are assigned a star formation duration of 4 Myr. We note that stellar feedback is not taken into account, and that stellar-feedback driven gas expulsion may terminate star formation at an earlier time than assumed here (e.g. Rahner et al. 2017; Kroupa et al. 2018). We impose a physical return time  $t_{\text{ret,fc0}} = 1$  Myr for the failed cores, as dictated by the time-span separating the ONC three stellar populations

**Table 2.** Input parameters  $\epsilon_{\text{ff,co}}$  and  $\rho_0$  for the models of Fig. 5.  $r_{\text{clump}} = 2$  pc,  $\epsilon_{\text{ff,st}} = 0.01$  and  $t_{\text{ret,fc0}} = 1$  Myr are imposed.  $m_{\text{st,4Myr}}$  is the stellar mass at  $t = 4$  Myr

| Model ID | $\epsilon_{\text{ff,co}}$ | $\rho_0$<br>[ $M_{\odot} \cdot \text{pc}^{-3}$ ] | $t_{\text{ret,fc0}}$<br>[ $\tau_{\text{ff},0}$ ] | $m_{\text{clump}}$<br>[ $M_{\odot}$ ] | $m_{\text{st,4Myr}}$<br>[ $M_{\odot}$ ] |
|----------|---------------------------|--|--|---------------------------------------|---|
| A1       | 0.10                      | $10^2$   | 1.2  | $3.3 \cdot 10^3$                      | $1.3 \cdot 10^2$                        |
| A2       | 0.10                      | $10^3$   | 3.9  | $3.3 \cdot 10^4$                      | $3.5 \cdot 10^3$                        |
| A3       | 0.10                      | $10^4$   | 12.4   | $3.3 \cdot 10^5$                      | $6.9 \cdot 10^4$                        |
| A4       | 0.10                      | $10^5$   | 39.1   | $3.3 \cdot 10^6$                      | $1.0 \cdot 10^6$                        |
| B1       | 0.30                      | $10^2$   | 1.2  | $3.3 \cdot 10^3$                      | $1.1 \cdot 10^2$                        |
| B2       | 0.30                      | $10^3$   | 3.9  | $3.3 \cdot 10^4$                      | $2.2 \cdot 10^3$                        |
| B3       | 0.30                      | $10^4$   | 12.4   | $3.3 \cdot 10^5$                      | $3.4 \cdot 10^4$                        |
| B4       | 0.30                      | $10^5$   | 39.1   | $3.3 \cdot 10^6$                      | $0.4 \cdot 10^6$                        |
| C1       | 0.50                      | $10^2$   | 1.2  | $3.3 \cdot 10^3$                      | $0.9 \cdot 10^2$                        |
| C2       | 0.50                      | $10^3$   | 3.9  | $3.3 \cdot 10^4$                      | $1.6 \cdot 10^3$                        |
| C3       | 0.50                      | $10^4$   | 12.4   | $3.3 \cdot 10^5$                      | $2.3 \cdot 10^4$                        |
| C4       | 0.50                      | $10^5$   | 39.1   | $3.3 \cdot 10^6$                      | $0.3 \cdot 10^6$                        |

(see Fig. 6 in Beccari et al. 2017). Combining the clump density with the physical return time of the failed cores provides their return time in units of the clump free-fall time  $t_{\text{ret,fc0}}/\tau_{\text{ff},0}$  (see Table 2). The return time of failed cores will be discussed further in Sec. 6. With  $t_{\text{ret,fc0}} = 1$  Myr and a star formation duration of 4 Myr, we expect our model star formation histories to present from 0 to 4 peaks, depending on the core formation efficiency per free-fall time  $\epsilon_{\text{ff,co}}$  and failed core return time  $t_{\text{ret,fc0}}/\tau_{\text{ff},0}$ .

The logarithmic stellar age distributions are presented in Fig. 5. The downward black arrows at an age of 5 Myr indicate the onset of core formation. Note in that respect the slight shift with the onset of the stellar age distribution, especially noticeable for the lowest-density models (i.e.  $\rho_0 = 100 M_{\odot} \cdot \text{pc}^{-3}$ ; red lines). This small shift corresponds to the time-delay  $t_{\text{ret,colco}} = 0.3\tau_{\text{ff},0}$  required by star-forming cores to shed their envelope in the intra-cluster medium (Eq. 11).

Figure 5 reveals that the presence of one peak per Myr for  $\geq 3$  Myr requires a clump density of at least  $\rho_0 \simeq 10^3 M_{\odot} \cdot \text{pc}^{-3}$  when the core formation efficiency per free-fall time is  $\epsilon_{\text{ff,co}} = 0.5$  (dashed green line in bottom panel). Lower core formation efficiencies per free-fall time must be "compensated" with higher initial gas densities (e.g.  $\rho_0 \simeq 10^5 M_{\odot} \cdot \text{pc}^{-3}$  when  $\epsilon_{\text{ff,co}} = 0.1$ , dashed magenta line in top panel). We note that models with a density similar to that of the present-day ONC (i.e.  $\rho_0 \simeq 10^2 M_{\odot} \cdot \text{pc}^{-3}$ ) fail to carve multiple peaks in their star formation history, irrespective of the adopted

core formation efficiency per free-fall time (solid red lines in all panels).

How can we disentangle between the models with  $\rho_0 = 10^3 M_\odot \cdot pc^{-3}$  and  $\epsilon_{ff,co} = 0.5$  and  $\rho_0 = 10^5 M_\odot \cdot pc^{-3}$  and  $\epsilon_{ff,co} = 0.1$  (models C2 and A4 in Table 2)? The initial gas mass  $m_{clump}$  and the stellar mass  $m_{st}$  at  $t = 4$  Myr constitute powerful tools here (see last two columns of Table 2). The C2 model ( $\rho_0 = 10^3 M_\odot \cdot pc^{-3}$  and  $\epsilon_{ff,co} = 0.5$ ) has formed  $1.6 \cdot 10^3 M_\odot$  in stars over 4 Myr (or  $1.4 \cdot 10^3 M_\odot$  over 3.3 Myr, which is the ONC star formation duration we will infer in the next section). This mass agrees much better with the current stellar content of the ONC ( $1800 M_\odot$ ; Hillenbrand & Hartmann 1998) than the stellar masses predicted with  $\rho_0 = 10^5 M_\odot \cdot pc^{-3}$ . Given the adopted radius  $r_{clump} = 2 pc$ , an initial gas density  $\rho_0 = 10^5 M_\odot \cdot pc^{-3}$  implies an initial gas mass of several million solar masses. This is 5 orders of magnitude higher than the mass of "ultra-high density material" detected by Hacar et al. (2020) in OMC-1 ( $\simeq 30 M_\odot$  at  $\simeq 10^5 M_\odot \cdot pc^{-3}$ ). The comparison of the observed gas and star masses to their model counterparts discards therefore the model A4. In other words, considering both the shape and normalisation of a star formation history allows one to disentangle whether the most appropriate model combines a high core formation efficiency per free-fall time to a low-density clump, or the other way round.

In the case of the ONC, we discard models with  $\rho_0 = 10^5 M_\odot \cdot pc^{-3}$  not just because of their too large gas and stellar masses, but also because the imposed physical return time  $t_{ret, fco} = 1$  Myr equates with  $t_{ret, fco} = 40\tau_{ff,0}$  ( $\tau_{ff,0} = 0.026$  Myr). Our model assumptions (e.g. constancy of the clump radius  $r_{clump}$ ) are unlikely to remain valid that long.

## 6. THE INTER-PEAK AGE-SPAN AS A DENSITY PROBE

A further observable which helps shed light on the initial gas density of a cluster-forming clump is the age span separating successive peaks of its stellar age distribution. Since high-density systems evolve faster than low-density ones, we intuitively expect the frequency of the peaks to be higher when the clump density is larger. Yet, we have so far assumed that the return time of failed cores  $t_{ret, fco}$  is independent of other model parameters. We now lift our assumption of a fixed return time  $t_{ret, fco} = 1$  Myr for the failed cores, and we relate  $t_{ret, fco}$  to the clump free-fall time  $\tau_{ff,0}$ , as already done for  $t_{ret, colco}$ , the time needed for star-forming cores to shed their envelope (Eq. 11).

### 6.1. The return time of the failed cores

Vázquez-Semadeni et al. (2005) infer an analytical estimate of how long it takes for a re-expanding core to double its radius, that is, to drop its mean density by almost an order of magnitude, when the external pressure exerted by the surrounding gas is negligible. We adopt this expansion time as a proxy to the failed core return time  $t_{ret, fco}$ . The left panel of Fig. 1 in Vázquez-Semadeni et al. (2005) shows that the return time  $t_{ret, fco}$  is in the following range

$$2 \frac{R_{eq}}{c_s} \lesssim t_{ret, fco} \lesssim 6 \frac{R_{eq}}{c_s}, \quad (16)$$

with  $R_{eq}$  the core equilibrium radius and  $c_s$  the core gas sound speed. The exact value depends on how far from equilibrium the core is following its initial compression. Since:

$$\frac{R_{eq}}{c_s} = \sqrt{\frac{\pi}{G\rho_{co}}} \quad (17)$$

for a core density  $\rho_{co}$  (e.g. Binney & Tremaine 1987), we can write<sup>2</sup>:

$$t_{ret, fco} = \Upsilon \sqrt{\frac{\pi}{G\rho_{fco}}} = \Upsilon \sqrt{\frac{32}{3}} \sqrt{\frac{3\pi}{32G\rho_{fco}}} = 3.3 \Upsilon \tau_{ff, fco} \quad (18)$$

with  $2 \lesssim \Upsilon \lesssim 6$ .

Now let us relate the mean density  $\rho_{fco}$  and free-fall time  $\tau_{ff, fco}$  of the failed cores to those of the host clump. According to Vázquez-Semadeni et al. (2005), core-to-cloud mean density ratios of  $\sim 30$ – $100$  yield gravitationally unstable cores when these are modeled as Bonnor-Ebert spheres. For our failed cores, we therefore adopt a weaker contrast  $\mathcal{C} = 10$  between their density  $\rho_{fco}$  and the host clump density  $\rho_0$ :

$$\mathcal{C} = \frac{\rho_{fco}}{\rho_0} = 10. \quad (19)$$

The free-fall time of failed cores then obeys  $\tau_{ff, fco} = \tau_{ff,0}/\sqrt{\mathcal{C}}$ , and we can modify Eq. 18 as

$$t_{ret, fco} = 3.3 \Upsilon \frac{\tau_{ff,0}}{\sqrt{\mathcal{C}}}. \quad (20)$$

With  $\mathcal{C} \simeq 10$ , the return time/re-expanding time of the failed cores becomes:

$$t_{ret, fco} \simeq \Upsilon \tau_{ff,0} \quad (21)$$

with  $2 \lesssim \Upsilon \lesssim 6$ .

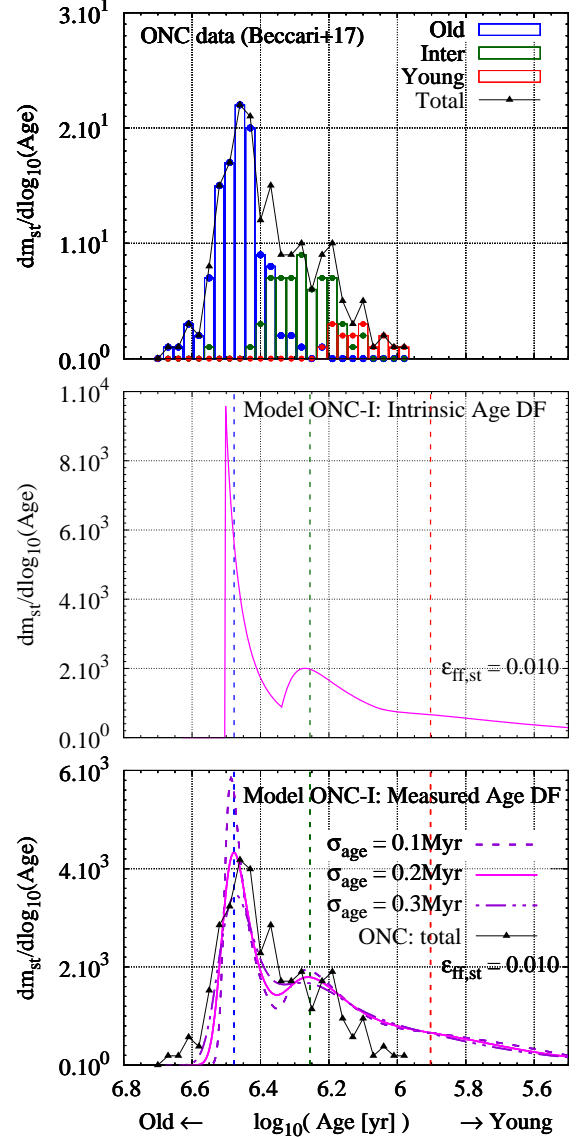
<sup>2</sup> It is worth noting here that Vázquez-Semadeni et al. (2005) adopt  $R_{eq}/c_s$  as their definition of the free-fall time, which is therefore longer than ours by a factor  $\sqrt{32/3}$ .

### 6.2. The ONC as a test-bed

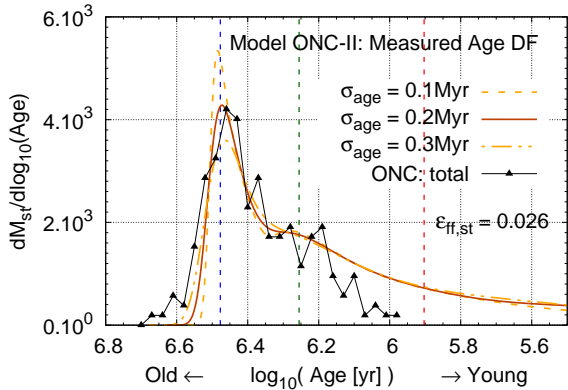
In Sec. 5, we have made a preliminary estimate of the initial gas density and free-fall time of the ONC progenitor, based on the 1 Myr star formation periodicity imposed by the observations. We have found:  $\rho_{clump}^{ONC} \simeq 10^3 M_{\odot} \cdot pc^{-3}$ , hence  $\tau_{ff,0}^{ONC} \simeq 0.26$  Myr. Does the corresponding  $\Upsilon$ -value make sense? Taking the 1-Myr timespan separating the successive stellar populations of the ONC as a proxy of the failed-core return time, we obtain  $\Upsilon \simeq t_{ret,fc}/\tau_{ff,0} \simeq 1 \text{ Myr}/0.26 \text{ Myr} \simeq 3.9$ , which falls in the range of viable  $\Upsilon$ -values quoted above. We conclude that the age-span between successive peaks of a stellar age distribution looks as a promising probe of the initial gas density. A prerequisite for this is that the return time of failed cores in units of the clump free-fall time, namely, the  $\Upsilon$  parameter (Eq. 21), is known. This topic obviously deserves more scrutiny, observations as well as simulations.

Figure 6 compares the observed age distribution of ONC pre-main sequence stars with a model with initial gas density  $\rho_0 = 10^3 M_{\odot} \cdot pc^{-3}$  and core formation efficiency per free-fall time  $\epsilon_{ff,co} = 0.50$ . The top panel shows the age distributions of the three stellar populations identified by Beccari et al. (2017), using the same color-coding as in their Fig. 6. Note that old ages are to the left and young ages (i.e. most recent star formation) are to the right. The black line with triangles is the total age distribution. Following the formation of the oldest population, the overall age distribution declines, highlighting a globally decreasing star formation rate as found for other star-forming regions (e.g. Chamaeleon I, Luhman 2007; Belloche et al. 2011b) and as predicted by Parmentier et al. (2014) (see also Preibisch 2012). We note that the three populations hardly show up when considering the total age distribution, an effect partly driven by stellar age uncertainties (see below).

The middle panel presents the model age distribution for  $\epsilon_{ff,co} = 0.5$ ,  $\rho_0 = 10^3 M_{\odot} \cdot pc^{-3}$  ( $m_{clump} = 3.35 \cdot 10^4 M_{\odot}$  and  $r_{clump} = 2 pc$ ), and an age of 3.3 Myr for the onset of core formation. Model parameters are quoted in Table 3 under "ONC-I". The model age distribution presents two well-distinct peaks, prolonged by a tail of lower star formation activity. The amplitude of the second peak is lower than that of the first/oldest one, as required to reproduce an overall decreasing star formation history. The mean ages of the old, intermediate and young populations as given by Beccari et al. (2017, their Table 1) are, respectively, 2.87, 1.88, and 1.24 Myr, with the individual stellar ages taken from Da Rio et al. (2016). More recent estimates of the three population mean ages (based on a different set of pre-main-sequence isochrones) are mentioned in Kroupa et al. (2018, their



**Figure 6.** Top panel: Logarithmic age distribution functions of the three populations of pre-main sequence stars identified by Beccari et al. (2017) in the ONC (blue, green and red histograms; see key). The sum of the three distributions is given by the black line with triangles. Middle panel: Logarithmic stellar age distribution function for the ONC-I model (parameters given in Table 3). The vertical blue, green and red dashed lines indicate the mean ages of the three populations as given in Kroupa et al. (2018). Bottom panel: Model age distribution function of the middle panel convolved by a Gaussian of standard deviation  $\sigma_{age}$  accounting for stellar age uncertainties. Results are presented for  $\sigma_{age} = 0.1, 0.2$  and  $0.3$  Myr (see key). The solid black line with triangles is the ONC total age distribution from the top panel normalized so as to present the same old-peak amplitude as the model with  $\sigma_{age} = 0.2$  Myr



**Figure 7.** Same as bottom panel of Fig. 6 but for the ONC-II model:  $m_{clump} = 10^4 M_{\odot}$ ,  $r_{clump} = 1.32$  pc,  $\epsilon_{ff,st} = 0.026$  and  $\epsilon_{ff,co} = 0.30$  (see also Table 3)

section 2.1) as 3.0, 1.8 and 0.8 Myr. These three ages are highlighted as the blue, green, and red vertical dashed lines, respectively. Note the shift of the youngest population towards even younger ages (i.e. shift between the red histogram in the top panel and the dashed red line in the middle panel). The most recent stellar population of the ONC would thus correspond to the trail of low-level star formation activity in the model of Fig. 6.

The bottom panel shows the impact of stellar age uncertainties. For this, we convolve the model output with a Gaussian function of standard deviation  $\sigma_{age}$ , with  $\sigma_{age}$  the uncertainty of individual stellar ages. The mean difference between the age estimates of the 3 populations as given by Beccari et al. (2017) and Kroupa et al. (2018) amounts to 0.2 Myr. We thus adopt  $\sigma_{age} = 0.2$  Myr. At an age of 1 Myr (3 Myr), this equates with a logarithmic age uncertainty  $\sigma_{\log_{10}age} = 0.09$  (0.03), in agreement with the uncertainties quoted in Table 5 of Da Rio et al. (2016). The convolved age distribution is given in the bottom panel of Fig. 6 as the solid magenta line. We also show the result for a larger ( $\sigma_{age} = 0.3$  Myr) or a smaller ( $\sigma_{age} = 0.1$  Myr) uncertainty (dash-dotted and dashed purple lines). At this stage, we refrain from a comprehensive browsing of the parameter space and from quantifying the fit quality with e.g. a  $\chi^2$ -test because of: (1) the uncertainties of the observed stellar age distribution at young ages, and (2) the absence of an initial gas density gradient in the current model. How a density gradient will qualitatively affect our results is discussed later in this section and in Sec. 7.4.

The relative amplitudes of the peaks of an *observed* star age distribution are of limited help to probe the history of a star-forming region. This is because the

**Table 3.** The ONC models of Sec. 6.2. Common parameters are:  $\rho_0 = 10^3 M_{\odot} \cdot pc^{-3}$ ,  $t_{ret,fc0} = 1$  Myr  $\equiv 3.9 \tau_{ff,0}$ , and an age of 3.3 Myr for core formation onset. Also given are the stellar mass and star formation efficiency at  $t = 3$  Myr

| Model ID | $m_{clump}$<br>[ $10^4 M_{\odot}$ ] | $\epsilon_{ff,co}$ | $\epsilon_{ff,st}$ | $m_{st,3Myr}$<br>[ $M_{\odot}$ ] | $SFE_{gl,3Myr}$ |
|----------|-------------------------------------|--------------------|--------------------|----------------------------------|-----------------|
| ONC-I    | 3.3                                 | 0.5                | 0.010              | 1400.                            | 0.04            |
| ONC-II   | 1.0                                 | 0.3                | 0.026              | 1500.                            | 0.15            |

peaks are unequally impacted by stellar age uncertainties. For instance, in our model, the first/oldest peak is the sharpest, thus the one most curtailed by stellar age uncertainties. A more robust indicator of the relative strengths of the successive star formation episodes is the stellar mass formed by each of them. The three populations identified by Beccari et al. (2017) contain, respectively, 111, 63 and 16 pre-main-sequence stars<sup>3</sup>. This is equivalent to 58%, 33% and 9% of the ONC stellar mass if the mean stellar mass is the same for all three populations, and if the observed samples are representative of their respective populations. The model-predicted fractions are more even, however, with 40%, 31.5% et 28.5% of the total stellar mass in the first, second and third million year, respectively. Adding an initial density gradient to the model clump will contribute to alleviating this (see Sec. 7.4). The total stellar mass produced by the model is  $1400 M_{\odot}$ , in rough agreement with that observed in the ONC ( $1800 M_{\odot}$ , Hillenbrand & Hartmann 1998).

The gas mass required by the ONC-I model may still seem prohibitive ( $m_{clump} = 3.35 \cdot 10^4 M_{\odot}$ ). It is higher by a factor  $\sim 3$  than any gas mass estimate proposed so far for the ONC progenitor (e.g.  $1.2 \cdot 10^4 M_{\odot}$ ; Kroupa et al. 2001). One parameter which can still be adjusted to reduce the initial gas mass and whose variations have not been explored yet is the star formation efficiency per free-fall time. By increasing  $\epsilon_{ff,st}$ , one can form a similar stellar mass out of a smaller amount of gas. Pokhrel et al. (2021) infer, as an average for 12 nearby molecular clouds,  $\epsilon_{ff,st} = 0.026$ . A model with  $\epsilon_{ff,st} = 0.026$  and  $\epsilon_{ff,co} = 0.30$  is shown in Fig. 7 (model ONC-II in Table 3). The clump mass and radius are, respectively,  $m_{clump} = 10^4 M_{\odot}$  and  $r_{clump} = 1.32$  pc (the radius has been decreased so as to retain the same den-

<sup>3</sup> Beccari et al. (2017) mention a census of 24 stars for the ONC youngest population. However, counting the number of objects in the red histogram of their Fig. 6 gives 16, and we use this latter number.

sity  $\rho_0$  as for the ONC-I model). The contributions in stars, star-forming core envelopes and failed cores to the core mass budget are provided in Table 1. The stellar mass formed after 3 Myr is  $m_{st} \simeq 1500 M_\odot$ , similar to that of the ONC-I model. The reason as to why a similar stellar mass forms out of a three-times smaller gas mass is two-fold here. Not only is the star formation efficiency per free-fall time  $\epsilon_{ff,st}$  higher ( $\epsilon_{ff,st} = 0.026$  vs.  $\epsilon_{ff,st} = 0.01$ ), the core formation efficiency per free-fall time  $\epsilon_{ff,co}$  is also smaller ( $\epsilon_{ff,co} = 0.30$  vs.  $\epsilon_{ff,co} = 0.50$ ), which has been shown in Fig. 4 to increase the clump star formation efficiency. Note that this latter effect comes at the expense of reducing the trough between the old and intermediate-age populations (compare the magenta and brown solid lines in bottom panel of Fig. 6 and Fig. 7, respectively).

Having used the observed stellar age distribution and stellar mass of the ONC to constrain the mass, density and core formation efficiency per free-fall time of its gaseous progenitor, it is tempting to compare our results with earlier studies. Kroupa et al. (2001) and Farias et al. (2020) study the kinematics of the ONC stars, including those unbound by gas expulsion and stellar interactions. The ONC model of Kroupa et al. (2001) builds on an initial gas mass of  $1.1 \cdot 10^4 M_\odot$  with a half-mass radius of  $r_{0.5} = 0.45$  pc, and a star formation efficiency of  $1/3$ . It gives rise to a bound cluster which retains one third of its initial stellar content in the aftermath of gas expulsion and survives for about 150 Myr. Our ONC-II model has a similar initial gas mass, but is more extended, the half-mass radius of our uniform density clump being  $1.32/2^{1/3} \simeq 1.05$  pc. A gas density gradient will make our model more compact, however. For instance, the same gas mass ( $m_{clump} = 10^4 M_\odot$ ) distributed inside the same radius ( $r_{clump} = 1.32$  pc) but according to a singular isothermal sphere yields an initial half-mass radius of  $r_{clump}/2 = 0.66$  pc for the gas. The stars will be even more concentrated (Parmentier & Pfalzner 2013). Another difference between ONC-II and Kroupa et al. (2001) is the global star formation efficiency  $SFE_{gl}$ . Kroupa et al. (2001) assume  $SFE_{gl} = 0.33$  at gas expulsion, while our model predicts  $SFE_{gl} = m_{st}/m_{clump} = 0.15$  at  $t = 3$  Myr. Does our low star formation efficiency imply that the ONC-II model cluster is unable to survive gas expulsion? Not once our model will include a gas density gradient. Stars will then form more centrally-concentrated than the embedding gas (Parmentier & Pfalzner 2013), and the locally higher star formation efficiency achieved by its inner regions will help the cluster retain part of its stars despite a globally low star formation efficiency (see also Adams 2000). Using  $N$ -body simula-

tions building on the model of Parmentier & Pfalzner (2013), Shukirgaliyev et al. (2017) conclude that the star formation efficiency threshold for cluster survival is  $SFE_{gl} = 0.15$ , with instantaneous gas expulsion and an external tidal field (taken as that of the Solar neighborhood). Not only will a gas density gradient help the cluster survive gas expulsion, it will also drive more efficient star formation (Parmentier 2019). This will raise  $SFE_{gl}$  above the threshold predicted by Shukirgaliyev et al. (2017), and reduce the initial gas mass  $m_{clump}$  accordingly (since the ONC stellar mass is imposed).

Farias et al. (2020) use their gradual cluster formation model (Farias et al. 2019) to model the velocity distribution function of the ONC stars, including run-aways and walk-aways. They conclude that slow star formation ( $\epsilon_{ff,st} = 0.01-0.03$ , rather than  $\epsilon_{ff,st} \geq 0.1$ ) and a progenitor clump surface density  $\Sigma_{clump} \simeq 7000 M_\odot \cdot pc^{-2}$  (rather than  $\Sigma_{clump} \simeq 700 M_\odot \cdot pc^{-2}$ ) provide the best match to the observations (their Fig. 10). The surface density of our ONC-II clump  $\Sigma_{clump} = 10^4/(\pi 1.32^2) \simeq 1800 M_\odot \cdot pc^{-2}$  is 4 times lower than what they advocate. Both models are not entirely comparable, however. While our star formation histories are intrinsically time-varying, Farias et al. (2019) assume a constant star formation rate fixed by the initial gas mass and free-fall time (their Eq. 7).

Although, in principle, the comparison of different modeling approaches should help cast more light on the formation and evolution of star clusters, this is no straightforward task, and the variety of model assumptions calls for a careful comparison.

### 6.3. Do observed single-population clusters hide multiple star formation episodes ?

The frequency at which cluster-forming clumps pile up successive star formation episodes now depends on the clump density  $\rho_0$  (Eqs 20 and 21). An interesting consequence is that the star formation histories of starburst clusters could have close-by peaks that, in the observed age distribution, get blended due to the short age-span separating them. To illustrate this possibility, let us consider two clumps with the same mass  $m_{clump} = 3.3 \cdot 10^5 M_\odot$ , radius  $r_{clump} = 2$  pc (i.e. clump density  $\rho_0 = 10^4 M_\odot \cdot pc^{-3}$ ) and star formation efficiency per free-fall time  $\epsilon_{ff,st} = 0.026$ , but distinct core formation efficiencies per free-fall time. With  $\epsilon_{ff,co} = 0.08$ , the first clump form no failed cores ( $F_{fco} = 0.0$ ; see Table 1 for  $\epsilon_{ff,st} = 0.026$ ). In contrast, with  $\epsilon_{ff,co} = 0.5$ , the second clump has a failed core mass fraction  $F_{fco} = 0.84$  (see Table 1). Their respective intrinsic stellar age distributions (Fig. 8) reflect this difference: a single spike when  $\epsilon_{ff,co} = 0.08$ , but 2-to-3 peaks for  $\epsilon_{ff,co} = 0.50$ .

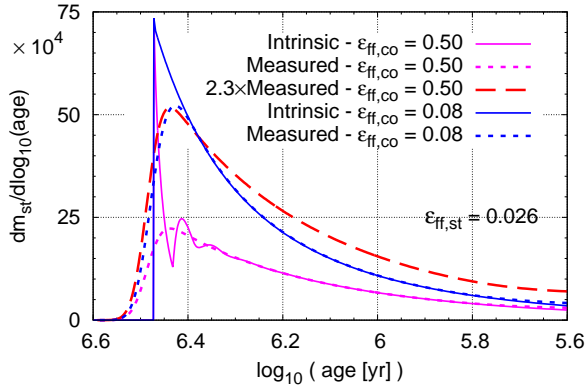


**Figure 8.** Intrinsic (solid lines) and measured (dashed lines) stellar age distributions for a cluster-forming clump with  $\rho_0 = 10^4 M_\odot \cdot pc^{-3}$ . The blue and magenta lines correspond to  $\epsilon_{ff,co} = 0.08$  and  $\epsilon_{ff,co} = 0.5$ , respectively (see key). The red long-dashed line is the measured age distribution for  $\epsilon_{ff,co} = 0.5$  raised to the same amplitude as for  $\epsilon_{ff,co} = 0.08$ : both measured age distributions are undistinguishable in shape

Note also the lower amplitude of the stellar distribution for  $\epsilon_{ff,co} = 0.50$ , which reflects the lower star formation efficiency induced by higher  $\epsilon_{ff,co}$ , as already noticed in Fig. 4.

The measured age distributions, that is, the intrinsic distributions convolved with a Gaussian error, tell a different story, however. We adopt  $\sigma_{age} = 0.2$  Myr, which is slightly smaller than what Kudryavtseva et al. (2012) inferred for the Galactic starburst cluster Westerlund 1 ( $\sigma_{age} = 0.25$  Myr). Given the very short clump free-fall time  $\tau_{ff,0} = 0.08$  Myr, the age span between two successive peaks is  $\simeq 0.3$  Myr ( $\Upsilon = 3.9$ ), and the multi-peak aspect shown by the  $\epsilon_{ff,co} = 0.50$  model is erased once stellar age uncertainties are accounted for (see magenta short-dashed line in Fig. 8). Figure 8 also shows as the red long-dashed line the measured age distribution for  $\epsilon_{ff,co} = 0.50$  normalized to the same maximum as for  $\epsilon_{ff,co} = 0.08$ . The shapes of both measured age distributions are hardly distinguishable, despite containing fundamentally different star formation histories.

Starburst clusters in the Galactic disk - like Westerlund 1 - are observed to be single-burst clusters (Kudryavtseva et al. 2012). The exercise above shows that the actual underlying star formation history may be quite different, however. We will revisit this issue in the future, once an initial gas density gradient will have been integrated into our model. The reader may indeed ask as to why the full-width at half-maximum of our convolved age distributions in Fig. 8 is as large as  $\simeq 1.5$  Myr, that is, significantly larger than the ob-

served full-width at half-maximum of 0.4 Myr inferred by Kudryavtseva et al. (2012) for Westerlund 1. This effect stems from the absence of an initial gas density gradient. A density gradient  $\rho_{gas} \propto r^{-2}$  will yield a full-width at half-maximum reduced by a factor 3-to-4 compared to a uniform density clump (see Fig. 4 in Parmentier 2019), thereby bringing model and observed full-widths at half-maximum in agreement.

## 7. DISCUSSION

### 7.1. Diversity in star-formation histories

Our model is able to generate very diverse star formation histories, from a star formation rate steadily decreasing with time to ‘jagged’ star formation histories. Additionally, the time-span between two successive peaks can vary from clump to clump, since it is a function of the initial gas density (Eq. 20).

Figure 5 seems to suggest that more numerous star formation episodes arise in denser and/or more massive clumps (in each panel, compare red solid and magenta dashed lines). This conclusion is erroneous, however. In each panel of Fig. 5, the varying parameter is the clump mass, while the clump radius and the *physical* return time of the failed cores are kept constant. Consequences are (1) a modification of the clump density  $\rho_0$ , hence of the clump free-fall time  $\tau_{ff,0}$  and, therefore, (2) a modification of the return time of the failed cores in units of the clump free-fall time  $t_{ret,fc}/\tau_{ff,0}$ . The seemingly greater ability of more massive clumps to carve more peaks in their star formation history in Fig. 5 stems from their failed core return time  $t_{ret,fc}/\tau_{ff,0}$  becoming longer by virtue of an increasingly shorter free-fall time  $\tau_{ff,0}$  coupled to a *constant physical return time*  $t_{ret,fc}$ . A longer return time of the failed cores  $t_{ret,fc}/\tau_{ff,0}$  allows a greater decrease of the gas density by the time failed cores disperse, yielding thereby a greater relative increase of the gas density and of the core formation rate at  $t \gtrsim t_{ret,fc}$ . In other words, to give the first core formation episode more time to subside increases the likelihood of the second core formation episode to spike (see also Sec. 2.2 and Fig. 3). Contrary to what a superficial glimpse at Fig. 5 may suggest, the initial gas mass has no influence on the shape of the core and star formation histories.

To illustrate this even more convincingly, let us consider a clump of mass  $m_{clump} = 3.3 \cdot 10^5 M_\odot$  and radius  $r_{clump} = 2$  pc (density  $\rho_0 = 10^4 M_\odot \cdot pc^{-3}$ ). We also consider three clumps with a 10-times higher mass and either (i) the same radius ( $m_{clump} = 3.3 \cdot 10^6 M_\odot$ ,  $r_{clump} = 2$  pc,  $\rho_0 = 10^5 M_\odot \cdot pc^{-3}$ ), or (ii) the same volume density ( $m_{clump} = 3.3 \cdot 10^6 M_\odot$ ,  $r_{clump} = 4.3$  pc,  $\rho_0 = 10^4 M_\odot \cdot pc^{-3}$ ), or (iii) the same surface den-

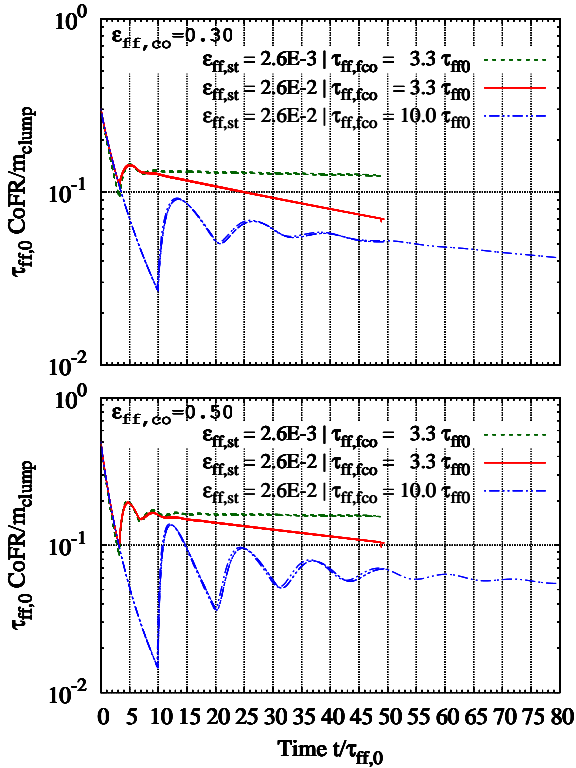


**Figure 9.** Evolution of the core formation rate normalized with the initial free-fall time  $\tau_{\text{ff},0}$  and initial mass  $m_{\text{clump}}$  of the clump gas, as a function of time after core formation onset in units of the clump free-fall time. Each line with given color and type corresponds to four model clumps with different masses  $m_{\text{clump}}$  and densities  $\rho_0$  (see text for details).

sity ( $m_{\text{clump}} = 3.3 \cdot 10^6 M_{\odot}$ ,  $r_{\text{clump}} = 6.3 \text{ pc}$ ,  $\rho_0 = 0.3 \cdot 10^4 M_{\odot} \cdot \text{pc}^{-3}$ ).

The mass  $m_{\text{clump}}$  and the density  $\rho_0$  define the *dimensional* parameters of the model. For each pair ( $m_{\text{clump}}$ ,  $\rho_0$ ), we vary the *dimensionless* model parameters, namely: the core formation efficiency per free-fall time  $\epsilon_{\text{ff},\text{co}}$ , the return time of the failed cores in units of the clump free-fall time  $t_{\text{ret},\text{fco}}/\tau_{\text{ff},0}$ , and the star formation efficiency per free-fall time  $\epsilon_{\text{ff},\text{st}}$ . We test the following values:  $\epsilon_{\text{ff},\text{co}} = (0.3, 0.5)$ ,  $t_{\text{ret},\text{fco}}/\tau_{\text{ff},0} = (3.3, 10.0)$ , and  $\epsilon_{\text{ff},\text{st}} = (0.0026, 0.026)$ . Twenty-four core formation histories are presented in Fig. 9 (top panel:  $\epsilon_{\text{ff},\text{co}} = 0.30$ ; bottom panel:  $\epsilon_{\text{ff},\text{co}} = 0.50$ ). Time on the  $x$ -axis is in units of the clump free-fall time, and the core formation rate on the  $y$ -axis is normalized by the initial mass and free-fall time of the gas. Models with a given set of dimensionless parameters (i.e. lines with given color and dashed type in a given panel) display identical normalized core formation histories. For instance, the 4 red solid lines, each depicting a ( $m_{\text{clump}}$ ,  $\rho_0$ )

combination, coincide with each other. The normalized core formation history  $\tau_{\text{ff},0} \text{CoFR}/m_{\text{clump}}(t/\tau_{\text{ff},0})$  is therefore independent of the clump mass  $m_{\text{clump}}$  and density  $\rho_0$ . It is shaped by the parameter triple ( $\epsilon_{\text{ff},\text{co}}, t_{\text{ret},\text{fco}}/\tau_{\text{ff},0}, \epsilon_{\text{ff},\text{st}}$ )<sup>4</sup>, while the clump mass and density (equivalently, the mass and free-fall time) act as scaling factors. A larger clump mass raises the core formation history without modifying its overall shape. A shorter free-fall time (i.e. denser clump) also provides a scaled-up version of the core formation history, while simultaneously increasing its "frequency".

For the parameters tested, Fig. 9 shows that we can expect up to 5-6 star formation episodes (for  $\epsilon_{\text{ff},\text{co}} = 0.50$  and  $t_{\text{ret},\text{fco}}/\tau_{\text{ff},0} = 10$ ). The choice of  $t_{\text{ret},\text{fco}}/\tau_{\text{ff},0} = 10$  for the return time of the failed cores may seem extreme. It requests  $\Upsilon \simeq 10$ , which goes beyond the range of values advocated in Sec. 6.1 (see Eqs 20-21). Yet,  $t_{\text{ret},\text{fco}}/\tau_{\text{ff},0} = 10$  may be relevant for environments where the external pressure is high enough to stabilize the cores for a longer time-span than when it is negligible (Lada et al. 2008).

Although the numbers of star formation episodes in Fig. 9 are comparable to the numbers of stellar populations identified in old globular clusters (often  $\geq 3$ -4 sub-populations; e.g. Carretta 2015; Bastian & Lardo 2018), we note that the relation between the two is not that straightforward (see Sec. 7.2)<sup>5</sup>.

The conclusion that the clump mass does not shape the core formation history seems at odd with what we know about old globular clusters, namely, that more massive globulars tend to present stronger multiple stellar population patterns. For instance, the mass of Galactic globular clusters correlates with their maximum helium abundance variation (Milone et al. 2018), with their maximum nitrogen abundance variation (Lagioia et al. 2019), and with the number fraction of stars enriched in hot hydrogen burning elements (Milone et al. 2017). Here, it is crucial to stress that the multiple stellar populations (generations if they fit a time sequence) of old globular clusters are identified based on their chemical abundances. In contrast, the

<sup>4</sup> For the sake of completeness, we should also mention the return time of the envelopes of star-forming cores  $t_{\text{ret},\text{colco}}/\tau_{\text{ff},0}$ . However, given that star-forming cores represent a minor fraction of the total core mass in models generating successive star formation episodes, this fourth dimensionless parameter is here of minor importance.

<sup>5</sup> An even greater number of stellar populations - 16 - have been extracted from the chromosome map of  $\omega$  Cen, the most massive Galactic globular cluster (Milone et al. 2017).  $\omega$  Cen, however, is likely the nucleus of a now disrupted dwarf galaxy (e.g. Hilker & Richtler 2000) and its early evolution cannot thus be explained with a cluster-based only scenario.



successive star formation episodes of our models are identified based on the star formation history and the failed core return time  $t_{ret, fco}$ .

The detailed star formation histories of old globular clusters have remained unknown so far, and our model does not compound the star formation history of a cluster with its chemical evolution. Yet, could our approach help shed light on as to why more massive globular clusters present more prominent multiple-stellar-population patterns?

### 7.2. Potential link with multiple stellar populations in old globular clusters

Patterns of multiple stellar populations vary greatly among Galactic old globular clusters. Specifically, the morphology of their chromosome map<sup>6</sup> is highly diverse - with no one cluster being identical to another. For instance, the branch of the so-called second generation is sometimes more clumpy (e.g. NGC2808), sometimes more continuous (e.g. NGC6652; see Fig. 4 in Milone et al. 2017). These maps also reveal varying numbers of globular cluster subpopulations. Similar conclusions can be drawn from the sodium-oxygen anticorrelation (see e.g. Fig. 1 in Charbonnel 2016). It is tempting to connect this aspect to our model star formation histories, whose aspect is sometimes 'wavy', with well-defined peaks and troughs (when  $\epsilon_{ff,co}$  and  $t_{retfco}/\tau_{H,0}$  are large), sometimes smoothly decreasing with time. But first, we have to cope with the apparent contradiction noted in Sec. 7.1, that high-mass globular clusters present the most striking patterns of multiple stellar populations and of enrichment in hot hydrogen burning elements, while the shape of our model star formation histories are independent of the progenitor clump mass (Fig. 9). Can we get out of this predicament?

Yes, if we assume that the stellar mass built by the clump must reach a given threshold  $m_{th}$  to trigger the formation of the polluters providing the hot hydrogen burning elements. This could be the case if the polluters are supermassive stars, namely, stars with masses a few  $10^3$  - a few  $10^4 M_{\odot}$  (Denissenkov & Hartwick 2014). Their predicted yields are in excellent agreement with the light-element abundance patterns observed in globular clusters (e.g. the sodium-oxygen anticorrelation: compare Fig. 1 in Charbonnel (2016) with the top-right panel of Fig. 1 in Denissenkov & Hartwick

(2014)). In addition, supermassive stars could pollute their environment during a few million years (Denissenkov & Hartwick 2014), similar to the time-span for cluster development. Their formation mechanism would be via stellar collisions, which requires either a high cluster density (e.g. Portegies Zwart et al. 2004), or a high number of stars (at least a few  $10^6$  stars; Gieles et al. 2018). Here, we build on the scenario that their formation requires a minimum number of stars, hence a minimum stellar mass  $m_{th}$ .

Let us consider three gas clumps (1,2,3) of mass  $m_1 < m_2 < m_3$ . The least massive clump is also less massive than the threshold mass  $m_{th}$ . With  $m_1 < m_{th}$ , clump 1 is unable to form a supermassive star, and the corresponding cluster does not display the light-element abundance variations typical of globular clusters. Yet, if the core formation efficiency  $\epsilon_{ff,co}$  and return time  $t_{ff,fco}/\tau_{H,0}$  of clump 1 are large enough, its star formation history does display successive star formation episodes. This may explain why open clusters do not present light-element abundance variations (MacLean et al. 2015), despite the fact that some (future) open clusters present multiple star formation episodes (e.g. the ONC, Beccari et al. 2017).

We now consider clump 2 and clump 3 as massive enough to form a supermassive star, i.e.  $m_{th} \ll m_2 < m_3$ . We also assume that their mass is the only parameter differentiating them (i.e. their free-fall times are equal, as well as their dimensionless parameters). With  $SFE_{2,th}$  and  $SFE_{3,th}$  the star formation efficiencies of clump 2 and clump 3 at the time they reach the stellar mass threshold  $m_{th}$ , we have  $SFE_{3,th} < SFE_{2,th}$  since  $m_{th} = SFE_{3,th}m_3 = SFE_{2,th}m_2$ . Because both clumps have identical free-fall times and dimensionless parameters, the growths with time of their respective star formation efficiencies are alike,  $SFE_2(t) = SFE_3(t)$ . Therefore, the inequality  $SFE_{3,th} < SFE_{2,th}$  implies that clump 3 reaches the threshold  $m_{th}$  at an earlier time than clump 2. This shift in time brings forward the formation of a supermassive star in clump 3, thereby providing a longer pollution time-span. As a result, the more massive clump should form a larger fraction of polluted stars, and achieve more extreme light-element abundance variations, as observed (Milone et al. 2017, 2018; Lagioia et al. 2019).

As long as the supermassive star does not "operate", newly-formed stars constitute the - chemically-defined - first stellar generation. We emphasize that the end of this generation coincides with the onset of the supermassive star pollution, not with the end of the first star formation episode of our model. If the intra-cluster medium pollution starts during the third star formation

<sup>6</sup> Chromosome maps trace multiple stellar populations based on their star *UV*-photometry. They build on the property that ultraviolet colors are very sensitive to star-to-star helium and light-element abundances (Milone et al. 2015)

episode, the first, second and beginning of third star formation episodes define the first stellar generation. Conversely, one could consider the case of a protoglobular clump with  $\epsilon_{\text{ff,co}} < 0.1$ , but massive enough to form a supermassive star. Its star formation history would be peakless (small core formation efficiency per free-fall time, hence small return fraction  $f_{\text{ret, fco}}$ ). Yet, the chromosome map would present two groups of stars corresponding to the stars born before and after the onset of the supermassive star pollution. In other words, the shape of the star formation history and the chemical evolution are decoupled from each other. While the shape of the star formation history depends on the model *dimensionless* parameters, the chemical evolution depends on a *dimensional* parameter (in the present case, the threshold stellar mass  $m_{\text{th}}$ ). This is the very reason as to why, all through this paper, we have refrained from using the term "stellar generations" to describe the successive star formation episodes of our model, this term being often used in studies of globular cluster multiple stellar populations. A consistent comparison between the number of star formation episodes predicted by our model and the number of multiple stellar generations in old globular clusters calls for a comparison between the return time of the failed cores with the chemical enrichment time-scale, which is beyond the scope of the present study.

Finally, we stress that the early evolution of globular clusters may see successive pollution episodes, driven by different polluters operating on different time-scales (e.g. D'Antona et al. 2016). Despite its low-mass ( $2.2 \cdot 10^4 M_{\odot}$ , Baumgardt et al. 2019), the globular cluster NGC6535 hosts two chemically-defined stellar populations (Milone et al. 2017). How could such a low-mass globular cluster contain stars bearing the imprint of hot hydrogen burning? Either the pollution of protoglobular clumps in hot hydrogen burning products is not caused by supermassive stars only. Or the current mass of NGC6535 is a tiny residual of a much larger initial mass. In either case, it is interesting to note that NGC6535 hosts two chemically-defined populations, while the much less massive ONC presents three star formation episodes. One more evidence that peaks in star formation histories are not direct matches to globular cluster multiple stellar generations.

### 7.3. Caveats and Limitations

Our idealized model does obviously not capture all aspects of the star formation process. In this section we assess its limitations and how more realistic conditions could affect its outcomes. We start by discussing our

assumption of an isolated clump in near-equilibrium (i.e. constant clump mass and radius).

The constancy of the clump radius constitutes a model central hypothesis since the gas density and core formation rate depend sensitively on it. Under what conditions can a cluster-forming clump remain in near-equilibrium once star formation has started? A key ingredient here is the feedback from forming stars, which stir their surrounding gas. Protostellar winds given off by low-mass stars were already suggested by Norman & Silk (1980) to be prime drivers of turbulence within molecular clouds. On the pc-scale of cluster-forming clumps, Nakamura & Li (2007) reach the same conclusion by means of hydrodynamical simulations. They show that even in case of fast turbulence decay, turbulence gets replenished from inside the clump due to the gas motions generated by protostellar outflows. This happens because protostellar outflows are collimated (i.e. bipolar outflows; see Bally 2016, for a review), allowing them to transport energy and momentum to greater distances from their sources than if they were spherically-symmetric (Nakamura & Li 2007). This "protostellar outflow-driven turbulence" allows the model clump of Nakamura & Li (2007) to remain close to dynamical equilibrium provided that the star formation efficiency per free-fall time amounts to a few per cent. There is in fact an interplay between the rates of turbulence decay and star formation. Matzner (2001) shows that a near-equilibrium configuration arises when turbulence decays slowly (over 10 free-fall times). When turbulence decays fast (over one free-fall time), however, continuous star formation is required for protostellar outflows to offset turbulence decay. If star formation happens discretely (i.e. one star at a time due to a low star formation rate), turbulence decay cannot be offset and the system collapses<sup>7</sup>. The star formation efficiency per free-fall time of our models ( $\epsilon_{\text{ff,st}} = 1\text{-}2.6\%$ ) is close to the limit for turbulence replenishment inferred by Nakamura & Li (2007) and, therefore, our assumption of a constant clump radius appears reasonable. Additionally, we note that even if our model had to include the contraction of a clump, this contraction is more likely to happen when the star formation rate reaches a low point, that is, one return time after a peak in the star formation history. Such a clump contraction would be timely to stimulate even more the rise of the next star formation episode by increasing the clump gas density.

<sup>7</sup> An example of a cluster-forming clump whose shrinking is unimpeded by protostellar outflows is provided in Huff & Stahler (2006).

One could now ask what the fate of these protostellar outflows is. Do they leave the cluster-forming clump (e.g. [Farias et al. 2019](#)), thereby decreasing the gas mass available to star formation, or do they remain trapped in the clump (our model). That is, how valid is the assumption of an isolated clump? This is a complex issue since it involves (1) the outflow speed and the clump escape velocity (hence the clump mass, radius, density profile, and the location of the source star inside the clump), and (2) the outflow morphology (which often consists of an inner high-velocity jet, superimposed to a slower wider-angle component, [Bally 2016](#)). The escaping outflows can also sweep part of the clump gas on their way out, thereby increasing the gas mass fraction lost from the clump. [Federrath et al. \(2014\)](#) find that more than a quarter of the clump mass can be ejected this way. On the one hand, the star formation rate would subside more quickly than predicted by our model, as a result of the corresponding gas mass decrease. On the other hand, additional star formation may be triggered since jets and outflows also drive local turbulent gas compressions ([Federrath et al. 2014](#)). Should the formation of failed cores be enhanced too, the multiple stellar population patterns predicted by our model will be strengthened. We also note that, when the leftover star-forming gas is completely expelled out of protoclusters due to massive star feedback, star formation may be triggered in the ensuing shell of expanding gas. This will add to the phenomenon of star cluster multiple stellar populations if the stellar component of the shell collapses back ([Parmentier 2004](#); [Rahner et al. 2018](#)).

Another way of modifying the mass enclosed within the adopted clump radius is by gas inflows. [Myers \(2009\)](#) find that all nine young stellar groups within 300 pc of the Sun radiate multiple filaments of parsec length, designing thereby a hub-filament structure. Gas flowing inwards along these filaments can fuel the cluster star formation process. This may be the case for the Serpens South embedded cluster ([Kirk et al. 2013](#)) and for the ONC ([Hacar et al. 2017a](#)). In the later case, [Hacar et al. \(2017a\)](#) estimate that the integral-shaped filament currently supplies the ONC with gas at a rate of  $\dot{M}_{acc} \simeq 385 M_{\odot} \cdot Myr^{-1}$ . This accretion rate cannot impact significantly the clump gas reservoir of our ONC-II model whose initial gas mass is  $10^4 M_{\odot}$ . This conclusion, however, would be different if the gas accretion rate was higher in the past ([Kroupa et al. 2018](#)). To assess the importance of filamentary accretion onto forming clusters cannot be performed without knowledge of the gas accretion rate history. In the case of our

model, the effect would be to fill in the troughs in the time evolution of the gas mass and, therefore, to reduce the amplitude of the oscillatory patterns seen in some of our simulations, which we now turn to.

Our model star formation histories can present clear-cut oscillations, which happens when failed cores dominate the core mass budget. These oscillations stem from the adoption, for each model clump, of a unique return time for all failed cores, i.e.  $t_{ret, fco} = 3.3\Upsilon_{ff,0}/\sqrt{\mathcal{C}}$  (with  $3.3\Upsilon$  the return time of the failed cores in unit of their free-fall time, and  $\mathcal{C}$  the core-to-clump mean density ratio; see Eqs 20, 19, 18). The amplitude of the oscillations as predicted by our model therefore constitutes an upper limit: in case of spatial variations in the core return time, the gas replenishment from simultaneously-formed cores is spread more evenly in time, smoothing thereby model oscillations. The effect would be especially significant for cores formed at a peak of core formation activity, since these cores bear the subsequent core formation history "upheaval". Although we have assumed that the clump gas remains uniform in density (albeit declining with time) through the clump evolution, it is not the case in practice. Hydrodynamical simulations of turbulent self-gravitating clouds produce filaments (e.g. [Federrath 2016](#); [Smith et al. 2016](#)), implying that the immediate environment of cores varies from one core to another, an effect also reinforced by spatial variations of the ram pressure arising from protostellar outflows ([Norman & Silk 1980](#)). With re-expanding cores confined by different external pressures, the  $\Upsilon$  parameter and, therefore, the return time  $t_{ret, fco}$  must vary from core to core. The mean density contrast  $\mathcal{C}$  of failed cores can also vary (although remaining markedly smaller than that of star-forming ones). More realistic simulations may thus show that the formation of clearly distinct star formation episodes is the exception rather than the rule, even when failed cores dominate the core mass budget by far. Interestingly, inspection of figures 3-7 in [Milone et al. \(2017\)](#) suggests that globular clusters whose enriched population draws a smooth distribution of points in the chromosome map outnumber those with clearly clumpy distributions (although photometric uncertainties contribute to this as well).

Another aspect that our present model does not account for is that of core coalescence (e.g. [Norman & Silk 1980](#); [Dib et al. 2010](#)). The corresponding mass increase may allow some of them to reach their Jeans mass, thereby turning failed cores into star-forming ones. This

too would reduce the amplitude of the star formation history oscillations.

Coalescence and return-time variations of failed cores contribute to explaining why the strong oscillatory patterns observed in some of our models do not show up in hydrodynamical simulations<sup>8</sup>: these are characterized by many more degrees of freedom than our model. But we also stress that such simulations need to cover at least 4-6 free-fall times of the modeled star-forming region for two subsequent oscillations to be uncovered.

Finally, a note about magnetic fields. The higher their initial strength in the cluster-forming clump, the lower the core formation efficiency per free-fall time (Dib et al. 2010). Magnetic field differences among cluster-forming clumps may thus contribute to whether or not subsequent star formation episodes emerge in clusters.

#### 7.4. Impact of an initial gas density gradient

In this contribution, we have restricted our attention to uniform density clumps. Yet, observed cluster-forming clumps are centrally-concentrated (e.g. Mueller et al. 2002). Compared to a top-hat profile, a gas density gradient strengthens the star formation activity of a clump by locating a greater fraction of its gas mass in its central regions, where the gas density is higher and the free-fall time shorter. To quantify this effect, Parmentier (2019) introduces the magnification factor  $\zeta$ , defined as the ratio between the star formation rate of a centrally-concentrated clump and that of its top-hat equivalent<sup>9</sup> (her equations 8-9; see also Tan et al. 2006). For instance, a gas density profile with a logarithmic slope of  $-2$  (Mueller et al. 2002) and a central plateau of extent  $10^{-2}$  the clump radius yields  $\zeta \simeq 2.5$  (see top panel in Fig. 1 of Parmentier & Pasquali 2020). The higher the gas density contrast between the clump center and the clump edge, the higher the magnification factor is, and the more invigorated star formation activity is.

In the framework of the present model, how would a density gradient affect our results? The star formation rate of a centrally-concentrated clump is given by Eq. 8 in Parmentier (2019), where  $\epsilon_{\text{ff,int}}$  is the intrinsic star formation efficiency per free-fall time, namely, the efficiency of the clump top-hat equivalent. The same equation can be rewritten as a core formation rate, by substituting the core formation efficiency per free-fall

time,  $\epsilon_{\text{ff,co}}$ , for the star formation efficiency per free-fall time  $\epsilon_{\text{ff,int}}$ :

$$CoFR_{clump} = \zeta \epsilon_{\text{ff,co}} \frac{m_{gas}}{\tau_{\text{ff}}} . \quad (22)$$

In this equation, the magnification factor  $\zeta$  can be associated either to the intrinsic core formation efficiency per free-fall time  $\epsilon_{\text{ff,co}}$

$$CoFR_{clump} = (\zeta \epsilon_{\text{ff,co}}) \frac{m_{gas}}{\tau_{\text{ff}}} , \quad (23)$$

or to the clump gas mass

$$CoFR_{clump} \propto \epsilon_{\text{ff,co}} \left( \frac{\zeta^{2/3} m_{gas}}{r_{clump}} \right)^{3/2} . \quad (24)$$

In the first case, the magnification factor raises the efficiency per free-fall time, implying that an initial gas density gradient strengthens the emergence of successive star formation episodes. In the second case, a given core formation rate can be achieved with a gas mass reduced by a factor  $\zeta^{2/3}$ . Equivalently, the clump star formation efficiency  $SFE_{gl}$  increases by a factor  $\zeta^{2/3}$ . For instance, the star formation efficiency of the ONC-II model ( $SFE_{gl} = 0.15$ , Sec. 6.2, Table 3) will be increased by a factor 1.6–2.1 if  $\zeta = 2-3$ .

We also expect a gas density gradient to modify the distribution of the stellar mass among the successive star formation episodes. The "weight" of the first/oldest star formation episode will increase at the expense of the subsequent ones, since the gas density contrast from clump center to clump edge plummets with time, causing in turn a decrease of the magnification factor (see Figs 2, 5 and 6 in Parmentier 2019).

We will investigate these aspects in future papers.

## 8. CONCLUSIONS

We have proposed a novel approach to understand the multiple stellar populations of star clusters. Our model hinges on the presence of failed cores in star-forming regions. Failed cores are density peaks of the interstellar medium which do not end collapsing and forming stars. Instead, they re-expand and disperse back in the inter-core gas. Although their existence has been known for more than two decades, both in observations (Taylor et al. 1996; Lada et al. 2008; Belloche et al. 2011a,b) and simulations (Clark & Bonnell 2005; Vázquez-Semadeni et al. 2005; Gómez et al. 2007), they have not received the same scrutiny as their star-forming counterparts. The formation of failed cores necessarily depletes the gas reservoir of a star-forming region. We therefore propose that their formation prompts the gas density, core and

<sup>8</sup> At least we are not aware of such simulations. Unfortunately, such publications do not always present their star or core formation history.

<sup>9</sup> The top-hat equivalent is a clump of uniform gas density containing the same gas mass as the centrally-concentrated clump, enclosed within the same radius.

star formation rates to dwindle. Their subsequent dispersion, however, allows the density of the surrounding gas to re-increase, thereby rejuvenating the core and star formation rates. When failed cores dominate the total core mass, this controlling mechanism of the available gas mass and density yields peaks and troughs in the time evolution of the gas density, hence of the core and star formation histories. The time-span on which failed cores disperse - which we coin their return time - determines the age-span separating the successive peaks of a star formation history.

Multiple peaks in the stellar age distribution of cluster-forming clumps (e.g. the ONC; [Beccari et al. 2017](#)) imply that a star formation episode must at some point recede, to allow the next one to rise. To implement the scenario described above, we therefore build on the volume-density driven cluster-formation model of [Parmentier & Pfalzner \(2013\)](#), which predicts a declining star formation activity in cluster-forming clumps under the assumptions of constant clump mass and size.

We start in Sec. 2 with a preliminary model in which star-forming and failed cores release their gas on the same time-scale. We find that three dimensionless parameters determine whether a core formation history unfolds at least two peaks: the core formation efficiency per free-fall time  $\epsilon_{\text{ff,co}}$ , the fraction  $f_{\text{return}}$  of the mass in cores that returns to the clump gas, and the associated time-span  $t_{\text{return}}/\tau_{\text{ff},0}$ , this one being expressed in units of the clump free-fall time  $\tau_{\text{ff},0}$ . High core formation efficiencies per free-fall time  $\epsilon_{\text{ff,co}}$ , high return fractions  $f_{\text{return}}$ , and long return times  $t_{\text{return}}/\tau_{\text{ff},0}$  favor the rise of a second core formation episode (see red-to-yellow areas in Fig. 3).

Following a review of the evidence for failed cores in observed and simulated star-forming regions in Sec. 3, we start to augment our model in Sec. 4. First, we introduce the star formation efficiency per free-fall time  $\epsilon_{\text{ff,st}}$ , whose combination with the core formation efficiency per free-fall time  $\epsilon_{\text{ff,co}}$  defines the respective fractions of the core mass turned into stars ( $F_*$ ), given off to the clump gas as star-forming core envelopes ( $F_{\text{env}}$ ), and as failed/rebounding cores ( $F_{\text{fco}}$ ) (see Eqs 13-15, and Table 1). Secondly, star-forming cores lose their envelope on a shorter time-span than failed cores disperse. We thus lift our assumption of identical return times for the failed cores and the star-forming core envelopes, and we assign them different time-scales (Eqs 11-12). We assume that failed cores disperse on a time-span  $t_{\text{ret,fco}} = 1$  Myr, which is the estimated life-expectancy of failed cores in the Pipe molecular cloud ([Lada et al. 2008](#)), and the core re-expansion time in the magneto-hydrodynamical simulations of [Vázquez-Semadeni et al.](#)

(2005). This is also the age-span separating the successive populations of pre-main sequence stars in the ONC ([Beccari et al. 2017](#)),

Next, in Sec. 5, we generate stellar age distributions for various clump masses and core formation efficiencies per free-fall time (Fig. 5). All model clumps are given the same star formation efficiency per free-fall time  $\epsilon_{\text{ff,st}}$ , radius  $r_{\text{clump}}$ , and physical return time  $t_{\text{ret,fco}} = 1$  Myr. Based on the number of peaks being carved in the star formation history with the imposed 1-Myr-periodicity and the corresponding stellar mass, we estimate that the ONC gaseous progenitor had a mean gas density  $\rho_0 = 10^3 M_{\odot} \cdot \text{pc}^{-3}$  and a core formation efficiency per free-fall time  $\epsilon_{\text{ff,co}} \geq 0.3$ . It bears repeating that this is the long return time of the failed cores  $t_{\text{ret,fco}}/\tau_{\text{ff},0}$  which drives the 'jagged' structure of the star formation history of the most massive clumps, *not* the clump mass itself.

In Sec. 6, we lift the assumption of a constant physical return time  $t_{\text{ret,fco}}$  for the failed cores. Using the analytical estimate of [Vázquez-Semadeni et al. \(2005, see left panel of their Fig. 1\)](#), we infer that the re-expanding time of failed cores amounts to a few free-fall times of their host clump (Eq. 21, with the free-fall time defined as in Eq. 2). We also propose two models for the star formation history of the ONC (Figs 6-7 and Table 3), and emphasize that the star formation history of starburst clusters may contain several star formation episodes, these remaining concealed (i.e. blended) due to their inter-peak age-span being comparable to stellar age uncertainties.

In Sec. 7, we discuss various aspects of our model. First, we emphasize the great diversity in the core and star formation histories we have generated. The *shapes* of the core and star formation histories depend on the dimensionless model parameters ( $t_{\text{ret,fco}}/\tau_{\text{ff},0}$ ,  $\epsilon_{\text{ff,co}}$ ,  $\epsilon_{\text{ff,st}}$ ). That is, the evolution of the normalized core formation rate  $\tau_{\text{ff},0} \text{CoFR}/m_{\text{clump}}$  as a function of time  $t/\tau_{\text{ff},0}$  depends exclusively on ( $t_{\text{ret,fco}}/\tau_{\text{ff},0}$ ,  $\epsilon_{\text{ff,co}}$ ,  $\epsilon_{\text{ff,st}}$ ) (Fig. 9). The *dimensional* parameters ( $m_{\text{clump}}$ ,  $\rho_0$ ) (i.e. clump mass and density) act as normalizing factors. Second, we discuss the potential relation between our model and the multiple stellar populations/generations ubiquitously observed in Galactic old globular clusters. That more massive globular clusters present stronger patterns of multiple stellar populations seems, at first sight, to contradict our finding of mass-independent star formation histories. Our star formation episodes, however, are defined based on the failed core return time, while the multiple stellar generations of old globular clusters are mapped based on their light-element abundances (e.g. chromosome map, [Milone et al. \(2015\)](#), and

sodium-oxygen anti-correlation, Carretta et al. (2010)). We qualitatively show that our model can produce massive clusters with a greater fraction of enriched stars if the formation of the stars polluting the cluster with hot hydrogen burning elements requires a threshold stellar mass. Third, we discuss the caveats and limitations of our model, emphasizing that more realistic conditions will smooth the strong oscillatory patterns carved in some of the predicted star formation histories. Finally, we discuss how the inclusion of a density gradient in our model clumps will impact our present results. We will

chart in greater depth these additional aspects, along with that of multiple stellar populations, in future papers.

GP acknowledges funding by the Deutsche Forschungsgemeinschaft (DFG, German Research Foundation – Project-ID 138713538 – SFB 881 (“The Milky Way System”, subproject B05)). This research has made use of NASA’s Astrophysics Data System. We thank the anonymous referee for a constructive report.

## REFERENCES

- Adams, F. C. 2000, *ApJ*, 542, 964. doi:10.1086/317052
- Alves, J., Lombardi, M., & Lada, C. J. 2007, *A&A*, 462, L17. doi:10.1051/0004-6361:20066389
- Anderson, J., Piotto, G., King, I. R., et al. 2009, *ApJL*, 697, L58. doi:10.1088/0004-637X/697/1/L58.
- André, P., Di Francesco, J., Ward-Thompson, D., et al. 2014, *Protostars and Planets VI*, 27. doi:10.2458/azu\_uapress\_9780816531240-ch002.
- Ballesteros-Paredes, J., André, P., Hennebelle, P., et al. 2020, *SSRv*, 216, 76. doi:10.1007/s11214-020-00698-3.
- Bally, J. 2016, *ARA&A*, 54, 491. doi:10.1146/annurev-astro-081915-023341.
- Bastian, N. & Lardo, C. 2018, *ARA&A*, 56, 83. doi:10.1146/annurev-astro-081817-051839
- Baumgardt, H., Hilker, M., Sollima, A., et al. 2019, *MNRAS*, 482, 5138. doi:10.1093/mnras/sty2997
- Beccari, G., Petr-Gotzens, M. G., Boffin, H. M. J., et al. 2017, *A&A*, 604, A22. doi:10.1051/0004-6361/201730432
- Belloche, A., Schuller, F., Parise, B., et al. 2011, *A&A*, 527, A145. doi:10.1051/0004-6361/201015733
- Belloche, A., Parise, B., Schuller, F., et al. 2011, *A&A*, 535, A2. doi:10.1051/0004-6361/201117276
- Binney, J. & Tremaine, S. 1987, *Princeton, N.J. : Princeton University Press*, c1987., p291
- Bonnor, W. B. 1956, *MNRAS*, 116, 351. doi:10.1093/mnras/116.3.351
- Carretta, E., Bragaglia, A., Gratton, R. G., et al. 2006, *A&A*, 450, 523. doi:10.1051/0004-6361:20054369.
- Carretta, E., Bragaglia, A., Gratton, R. G., et al. 2010, *A&A*, 516, A55. doi:10.1051/0004-6361/200913451.
- Carretta, E. 2015, *ApJ*, 810, 148. doi:10.1088/0004-637X/810/2/148
- Clark, P. C. & Bonnell, I. A. 2005, *MNRAS*, 361, 2. doi:10.1111/j.1365-2966.2005.09105.x.
- Charbonnel, C. 2016, *EAS Publications Series*, 80-81, 177. doi:10.1051/eas/1680006
- Cordoni, G., Milone, A. P., Marino, A. F., et al. 2018, *ApJ*, 869, 139. doi:10.3847/1538-4357/aaedc1
- Da Rio, N., Tan, J. C., Covey, K. R., et al. 2016, *ApJ*, 818, 59. doi:10.3847/0004-637X/818/1/59.
- Da Rio, N., Tan, J. C., Covey, K. R., et al. 2017, *ApJ*, 845, 105. doi:10.3847/1538-4357/aa7a5b.
- D’Antona, F., Caloi, V., Montalbán, J., et al. 2002, *A&A*, 395, 69. doi:10.1051/0004-6361:20021220.
- D’Antona, F., Vesperini, E., D’Ercole, A., et al. 2016, *MNRAS*, 458, 2122. doi:10.1093/mnras/stw387
- Denissenkov, P. A. & Hartwick, F. D. A. 2014, *MNRAS*, 437, L21. doi:10.1093/mnrasl/slt133
- D’Ercole, A., Vesperini, E., D’Antona, F., et al. 2008, *MNRAS*, 391, 825. doi:10.1111/j.1365-2966.2008.13915.x
- Decressin, T., Charbonnel, C., & Meynet, G. 2007, *A&A*, 475, 859. doi:10.1051/0004-6361:20078425.
- D’Ercole, A., Vesperini, E., D’Antona, F., et al. 2008, *MNRAS*, 391, 825. doi:10.1111/j.1365-2966.2008.13915.x.
- Dib, S., Hennebelle, P., Pineda, J. E., et al. 2010, *ApJ*, 723, 425. doi:10.1088/0004-637X/723/1/425
- Dupree, A. K., Dotter, A., Johnson, C. I., et al. 2017, *ApJL*, 846, L1. doi:10.3847/2041-8213/aa85dd
- Galván-Madrid, R., Vázquez-Semadeni, E., Kim, J., et al. 2007, *ApJ*, 670, 480. doi:10.1086/522081
- Gómez, G. C., Vázquez-Semadeni, E., Shadmehri, M., et al. 2007, *ApJ*, 669, 1042. doi:10.1086/521620.
- Farias, J. P., Tan, J. C., & Eyer, L. 2020, *ApJ*, 900, 14. doi:10.3847/1538-4357/aba699
- Farias, J. P., Tan, J. C., & Chatterjee, S. 2019, *MNRAS*, 483, 4999. doi:10.1093/mnras/sty3470
- Federrath, C., Schrön, M., Banerjee, R., et al. 2014, *ApJ*, 790, 128. doi:10.1088/0004-637X/790/2/128.
- Federrath, C. 2016, *MNRAS*, 457, 375. doi:10.1093/mnras/stv2880.
- Gieles, M., Charbonnel, C., Krause, M. G. H., et al. 2018, *MNRAS*, 478, 2461. doi:10.1093/mnras/sty1059.

- Hacar, A., Tafalla, M., & Alves, J. 2017, *A&A*, 606, A123. doi:10.1051/0004-6361/201630348
- Hacar, A., Hogerheijde, M. R., Harsono, D., et al. 2020, *A&A*, 644, A133. doi:10.1051/0004-6361/202038138.
- Hatchell, J., Richer, J. S., Fuller, G. A., et al. 2005, *A&A*, 440, 151. doi:10.1051/0004-6361:20041836.
- Hilker, M. & Richtler, T. 2000, *A&A*, 362, 895.
- Hillenbrand, L. A. & Hartmann, L. W. 1998, *ApJ*, 492, 540. doi:10.1086/305076.
- Huff, E. M. & Stahler, S. W. 2006, *ApJ*, 644, 355. doi:10.1086/503357.
- Kainulainen, J., Federrath, C., & Henning, T. 2014, *Science*, 344, 183. doi:10.1126/science.1248724
- Keto, E., Broderick, A. E., Lada, C. J., et al. 2006, *ApJ*, 652, 1366. doi:10.1086/508251
- Kirk, H., Myers, P. C., Bourke, T. L., et al. 2013, *ApJ*, 766, 115. doi:10.1088/0004-637X/766/2/115
- Klessen, R. S. 2001, *ApJ*, 556, 837. doi:10.1086/321626.
- Kraft, R. P. 1994, *PASP*, 106, 553. doi:10.1086/133416.
- Kroupa, P., Aarseth, S., & Hurley, J. 2001, *MNRAS*, 321, 699. doi:10.1046/j.1365-8711.2001.04050.x
- Kroupa, P., Jeřábková, T., Dinnbier, F., et al. 2018, *A&A*, 612, A74. doi:10.1051/0004-6361/201732151.
- Krumholz, M. R. & Tan, J. C. 2007, *ApJ*, 654, 304. doi:10.1086/509101
- Kudryavtseva, N., Brandner, W., Gennaro, M., et al. 2012, *ApJL*, 750, L44. doi:10.1088/2041-8205/750/2/L44
- Lada, C. J., Muench, A. A., Rathborne, J., et al. 2008, *ApJ*, 672, 410. doi:10.1086/523837.
- Lagioia, E. P., Milone, A. P., Marino, A. F., et al. 2019, *AJ*, 158, 202. doi:10.3847/1538-3881/ab45f2.
- Langer, G. E., Hoffman, R., & Sneden, C. 1993, *PASP*, 105, 301. doi:10.1086/133147
- Luhman, K. L. 2007, *ApJS*, 173, 104. doi:10.1086/520114
- Matzner, C. D. & McKee, C. F. 2000, *ApJ*, 545, 364. doi:10.1086/317785
- Matzner, C. D. 2001, *From Darkness to Light: Origin and Evolution of Young Stellar Clusters*, 243, 757.
- MacLean, B. T., De Silva, G. M., & Lattanzio, J. 2015, *MNRAS*, 446, 3556. doi:10.1093/mnras/stu2348
- Marino, A. F., Milone, A. P., Casagrande, L., et al. 2018, *ApJL*, 863, L33. doi:10.3847/2041-8213/aad868.
- Milone, A. P., Bedin, L. R., Piotto, G., et al. 2008, *ApJ*, 673, 241. doi:10.1086/524188.
- Milone, A. P., Marino, A. F., Piotto, G., et al. 2015, *ApJ*, 808, 51. doi:10.1088/0004-637X/808/1/51.
- Milone, A. P., Piotto, G., Renzini, A., et al. 2017, *MNRAS*, 464, 3636. doi:10.1093/mnras/stw2531.
- Milone, A. P., Marino, A. F., Renzini, A., et al. 2018, *MNRAS*, 481, 5098. doi:10.1093/mnras/sty2573
- Mueller, K. E., Shirley, Y. L., Evans, N. J., et al. 2002, *ApJS*, 143, 469. doi:10.1086/342881
- Myers, P. C. 2009, *ApJ*, 700, 1609. doi:10.1088/0004-637X/700/2/1609.
- Nakamura, F. & Li, Z.-Y. 2007, *ApJ*, 662, 395. doi:10.1086/517515.
- Norman, C. & Silk, J. 1980, *ApJ*, 238, 158. doi:10.1086/157969
- Oliveira, R. A. P., Souza, S. O., Kerber, L. O., et al. 2020, *ApJ*, 891, 37. doi:10.3847/1538-4357/ab6f76
- Parmentier, G. 2004, *MNRAS*, 351, 585. doi:10.1111/j.1365-2966.2004.07804.x.
- Parmentier, G. & Pfalzner, S. 2013, *A&A*, 549, A132. doi:10.1051/0004-6361/201219648.
- Parmentier, G., Pfalzner, S., & Grebel, E. K. 2014, *ApJ*, 791, 132. doi:10.1088/0004-637X/791/2/132.
- Parmentier, G. 2019, *ApJ*, 887, 179. doi:10.3847/1538-4357/ab53d6
- Parmentier, G. & Pasquali, A. 2020, *ApJ*, 903, 56. doi:10.3847/1538-4357/abb8d3.
- Piotto, G., Bedin, L. R., Anderson, J., et al. 2007, *ApJL*, 661, L53. doi:10.1086/518503.
- Pokhrel, R., Gutermuth, R. A., Krumholz, M. R., et al. 2021, arXiv:2104.04551
- Portegies Zwart, S. F., Baumgardt, H., Hut, P., et al. 2004, *Nature*, 428, 724. doi:10.1038/nature02448
- Prantzos, N. & Charbonnel, C. 2006, *A&A*, 458, 135. doi:10.1051/0004-6361:20065374.
- Preibisch, T. 2012, *Research in Astronomy and Astrophysics*, 12, 1. doi:10.1088/1674-4527/12/1/001.
- Rahner, D., Pellegrini, E. W., Glover, S. C. O., et al. 2017, *MNRAS*, 470, 4453. doi:10.1093/mnras/stx1532.
- Rahner, D., Pellegrini, E. W., Glover, S. C. O., et al. 2018, *MNRAS*, 473, L11. doi:10.1093/mnras/slx149.
- Schneider, F. R. N., Ramírez-Agudelo, O. H., Trammer, F., et al. 2018, *A&A*, 618, A73. doi:10.1051/0004-6361/201833433
- Shukirgaliyev, B., Parmentier, G., Berczik, P., et al. 2017, *A&A*, 605, A119. doi:10.1051/0004-6361/201730607
- Smith, R. J., Glover, S. C. O., Klessen, R. S., et al. 2016, *MNRAS*, 455, 3640. doi:10.1093/mnras/stv2559
- Tan, J. C., Beltrán, M. T., Caselli, P., et al. 2014, *Protostars and Planets VI*, 149. doi:10.2458/azu\_uapress\_9780816531240-ch007
- Tan, J. C., Krumholz, M. R., & McKee, C. F. 2006, *ApJL*, 641, L121. doi:10.1086/504150.
- Taylor, S. D., Morata, O., & Williams, D. A. 1996, *A&A*, 313, 269
- Vázquez-Semadeni, E., Kim, J., Shadmehri, M., et al. 2005, *ApJ*, 618, 344. doi:10.1086/425951.

Ward-Thompson, D., André, P., Crutcher, R., et al. 2007,  
Protostars and Planets V, 33